(12) INTERNATIONAL APPLICATION PUBLISHED UNDER THE PATENT COOPERATION TREATY (PCT)

(19) World Intellectual Property Organization
International Bureau

(43) International Publication Date
22 November 2018 (22.11.2018)

WIPO | PCT

(10) International Publication Number
WO 2018/210334 A1

(51) International Patent Classification:
C07D 215/42 (2006.01) *C09K 11/06* (2006.01)
C07D 215/26 (2006.01) *G01N 21/64* (2006.01)
C07D 213/30 (2006.01) *A61P 31/04* (2006.01)
A61K 31/44 (2006.01) *A61P 35/00* (2006.01)
A61K 31/438 (2006.01)

(21) International Application Number:
PCT/CN2018/087479

(22) International Filing Date:
18 May 2018 (18.05.2018)

(25) Filing Language: English

(26) Publication Language: English

(30) Priority Data:
62/603,131 19 May 2017 (19.05.2017) US

(71) Applicant: **THE HONG KONG UNIVERSITY OF SCIENCE AND TECHNOLOGY** [CN/CN]; Clear Water Bay, Kowloon, Hong Kong (CN).

(72) Inventors: **TANG, Benzhong**; c/o The Hong Kong University of Science and Technology, Clear Water Bay, Kowloon, Hong Kong (CN). **KANG, Miaomiao**; c/o The Hong Kong University of Science and Technology, Clear Water Bay, Kowloon, Hong Kong (CN). **GU, Xinggui**; c/o The Hong Kong University of Science and Technology, Clear Water Bay, Kowloon, Hong Kong (CN).

(74) Agent: **TEE & HOWE INTELLECTUAL PROPERTY ATTORNEYS**; DING, Yeping, 10th Floor, Tower D, Minsheng Financial Center, 28 Jianguomennei Avenue, Dongcheng District, Beijing 100005 (CN).

(81) Designated States *(unless otherwise indicated, for every kind of national protection available)*: AE, AG, AL, AM, AO, AT, AU, AZ, BA, BB, BG, BH, BN, BR, BW, BY, BZ, CA, CH, CL, CN, CO, CR, CU, CZ, DE, DJ, DK, DM, DO, DZ, EC, EE, EG, ES, FI, GB, GD, GE, GH, GM, GT, HN, HR, HU, ID, IL, IN, IR, IS, JO, JP, KE, KG, KH, KN, KP, KR, KW, KZ, LA, LC, LK, LR, LS, LU, LY, MA, MD, ME, MG, MK, MN, MW, MX, MY, MZ, NA, NG, NI, NO, NZ, OM, PA, PE, PG, PH, PL, PT, QA, RO, RS, RU, RW, SA, SC, SD, SE, SG, SK, SL, SM, ST, SV, SY, TH, TJ, TM, TN, TR, TT, TZ, UA, UG, US, UZ, VC, VN, ZA, ZM, ZW.

(84) Designated States *(unless otherwise indicated, for every kind of regional protection available)*: ARIPO (BW, GH, GM, KE, LR, LS, MW, MZ, NA, RW, SD, SL, ST, SZ, TZ, UG, ZM, ZW), Eurasian (AM, AZ, BY, KG, KZ, RU, TJ, TM), European (AL, AT, BE, BG, CH, CY, CZ, DE, DK, EE, ES, FI, FR, GB, GR, HR, HU, IE, IS, IT, LT, LU, LV, MC, MK, MT, NL, NO, PL, PT, RO, RS, SE, SI, SK, SM, TR), OAPI (BF, BJ, CF, CG, CI, CM, GA, GN, GQ, GW, KM, ML, MR, NE, SN, TD, TG).

Published:
— *with international search report (Art. 21(3))*

WO 2018/210334 A1

(54) Title: AIEGENS FOR CANCER CELLS AND GRAM-POSITIVE BACTERIA DISCRIMINATION AND KILLING

(57) Abstract: AIE luminogens as theranostic agents may be used in photodynamic therapy to selectively detect and kill cancer cells and gram-positive bacteria. The theranostic agent can include a small molecule, organic compound capable of aggregation-induced emission and generation of reactive oxygen species upon exposure to white light. The theranostic agent may be used to selectively visualize and/or impair or stop the growth of cancer cells or Gram-positive bacteria in situ during a surgical procedure.

AIEgens for Cancer Cells and Gram-Positive Bacteria Discrimination and Killing

CROSS-REFERENCE

The present application claims priority to provisional United States Patent Application No. 62/603,131, filed May 19, 2017, which was filed by the inventors hereof and is incorporated herein by reference in its entirety.

FIELD

The present subject matter relates generally to the synthesis of luminogens with aggregation-induced emission (AIE) characteristics and their applications as fluorescent probes for cancer cell and Gram-positive bacteria imaging and selective killing.

BACKGROUND

The emergence of photo-theranostic agents has opened a new door for cancer research. Theranostic agents can facilitate integration of real-time diagnosis and *in-situ* phototherapeutic capabilities in one platform. Diagnosis of cancer at early stages of the disease is difficult due to the small size of most early stage tumors. Therefore, high selectivity and sensitivity are of great importance for both early diagnosis of cancer and investigation of cancer metastasis.

Bacteria are intimately related to human life in many aspects. Most bacteria are benign, some of which are probiotic and beneficial to human beings. However, a few species of bacteria will cause infections and even induce serious diseases which are harmful or even fatal for human bodies. For example, well-known bacteria such as *Escherichia coli* (*E. coli*, Gram-negative bacteria) when in our intestinum crassum can produce vitamin B and K, thus a certain amount of *E. coli* is necessary for maintaining normal physiological functions of our body. *Staphylococcus aureus* (*S. aureus*, Gram-positive bacteria), anotorious pathogenic bacteria, generate enterotoxin which can lead to acute gastroenteritis. Therefore, the development of simple and rapid methods for discriminating probiotic against pathogenic bacteria and selectively kill the pathogenic bacteria is of great significance in bacterial-related diseases.

The living body is a comprehensive system, in which cells and bacteria are always present. For example, in asurgical operation process, which is a common approach to remove tumors, infection often occurs and is defined as surgical site infection (SSI). SSI has attracted public interest and clinical researcher. To date, diagnostic tests, including ultrasound, X-ray, photoacoustic, computed tomography, positron emission tomography, and magnetic resonance

imaging have been commonly used in the detection of cancer. On the other hand, techniques involving Gram staining after direct smear methods or isolation culture and identification have been developed and widely used exclusively for bacteria detection.

Compared to conventional imaging techniques, fluorescence imaging possesses the advantages of superb sensitivity, good accessibility, low cost, and reliable safety. Furthermore, a considerable number of fluorescence imaging agents are suitable for theranostic applications, as they can undergo photophysical and photochemical processes under light irradiation to generate toxic reactive oxygen species (ROS) *in situ*, which is widely used for photodynamic therapy (PDT) in tumor ablation. However, the most-widely used materials for PDT, such as porphyrin and phenothiazium, suffer from detrimental aggregation-caused quenching (ACQ), which leads to low photobleaching resistance and finite ROS production. This results in low therapeutic efficiency and greatly impedes the practical application of these materials as theranostic agents.

Recently, compounds demonstrating aggregation-induced emission (AIE),a phenomenonopposite to the ACQ effect, have been developed. Luminogens with AIE characteristics (AIEgens) are weakly emissive when dissolved in solution, but show fluorescence in the aggregate state. This feature endows AIEgens with the intrinsic capacity to work perfectly at high concentrations or in the aggregate state with bright fluorescence and a high photobleaching threshold. Furthermore, some AIEgen-based probes also exhibit effective ROS generation in the aggregate state.

Therefore, AIE luminogen probes as theranostic agents for cancer and Gram-positive bacteria detection and killing are desired.

SUMMARY

The present subject matter relates to AIE luminogen probes that can be used as theranostic agents. The theranostic agents can be used for the selective imaging and killing of harmful cells. The harmful cells can include cancer cells and gram-positive bacteria. The theranostic agents can be administered to a patient undergoing a surgical procedure in order to selectively identify and/or kill harmful cells. The theranostic agent may in administered *in situ* at the site of the surgical procedure. The theranostic agent may allow selective imaging of cancer cells and/or Gram-positive bacteria through AIE mediated fluorescence. The theranostic agent may be used in photodynamic therapy to kill or impair the growth of the harmful cells by exposure of the theranostic agent to white light. In this regard, the theranostic agent can be

administered to a patient to locate a site of harmful cells in the patient using fluorescent imaging. Once the site of the harmful cells has been determined, the site can be irradiated with white light which, when combined with the present compounds, can stop or inhibit the growth of the harmful cells.

In an embodiment, the present AIE luminogen probe is a small molecule, organic compound that has a chemical structure selected from the group consisting of:

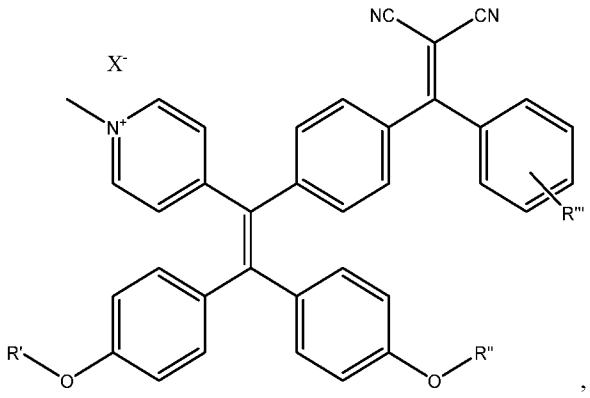

,

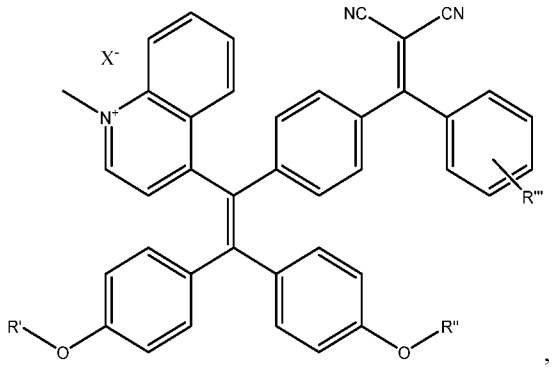

,

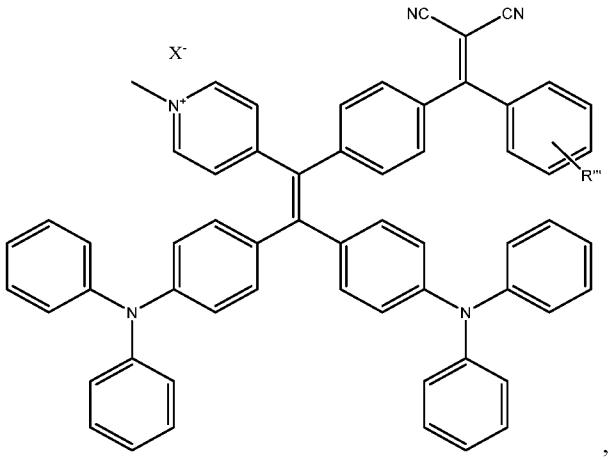

,

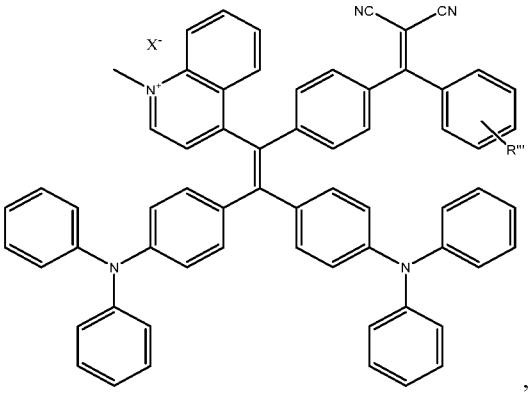

,

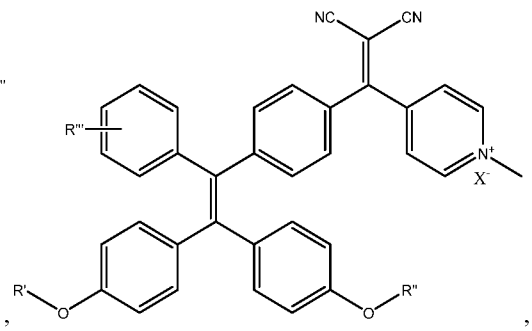

,

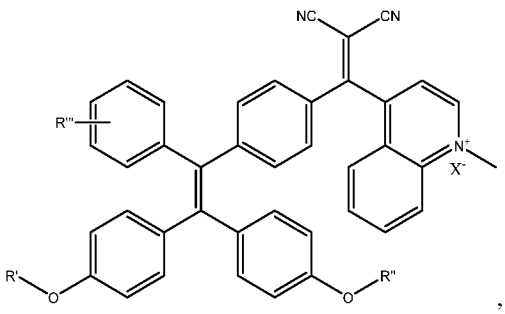

,

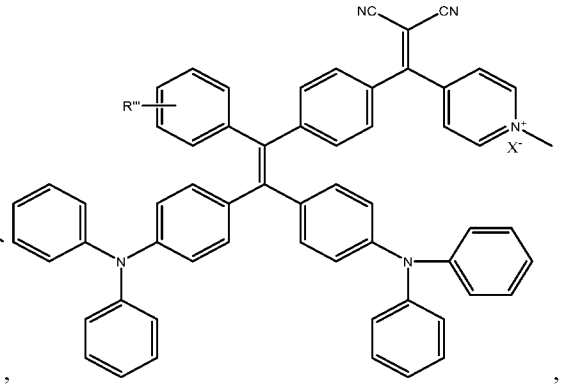

, and

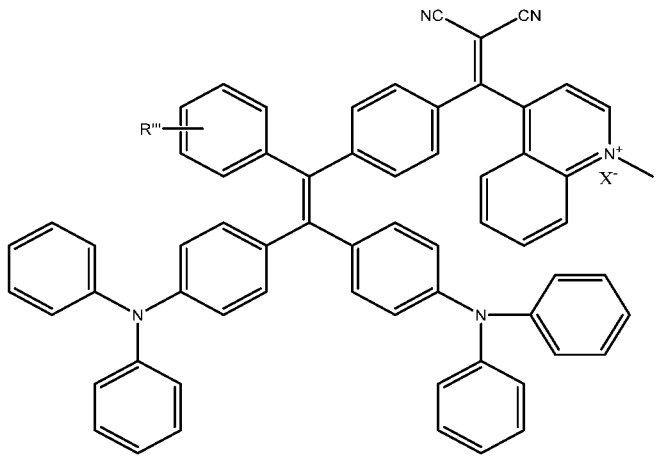

;

wherein R', R", and R"' are independently selected from the group consisting of H, alkyl, unsaturated alkyl, heteroalkyl, cycloalkyl, heterocycloalkyl, aryl, heteroaryl, alkyl-NCS, alkyl-N_3, and alkyl-NH_2; and

wherein the counteranion X^- is selected from the group consisting of I^-, PF_6^-, BF_4^-, SbF_6^-, SbF_5^-,

CH_3COO^-, CF_3COO^-, CO_3^{2-}, SO_4^{2-}, SO_3^{2-}, $CF_3SO_2^-$, TsO^-, ClO_4^-, F^-, Cl^-, Br^-, $(F_3CSO_2)N^-$, and PO_4^{3-}.

In a further embodiment, the compound has a chemical structure selected from the group consisting of:

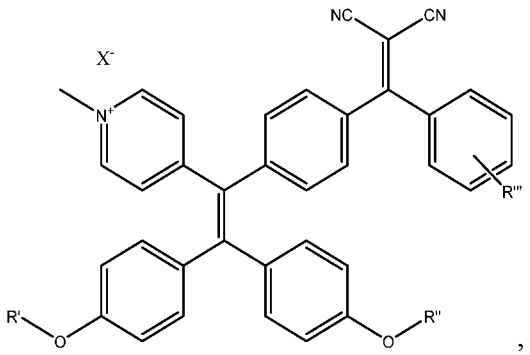

, and

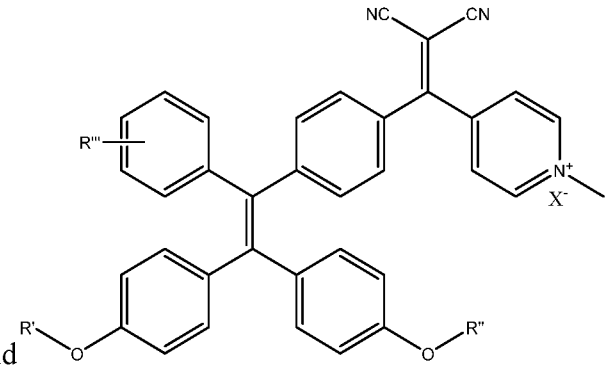

;

wherein R', R", and R"' are independently selected from the group consisting of H, alkyl, unsaturated alkyl, heteroalkyl, cycloalkyl, heterocycloalkyl, aryl, heteroaryl, alkyl-NCS, alkyl-N_3, and alkyl-NH_2; and

wherein the counteranion X^- is selected from the group consisting of I^-, PF_6^-, BF_4^-, and SbF_6^-.

In an embodiment, the compound has one of the following structural formulae:

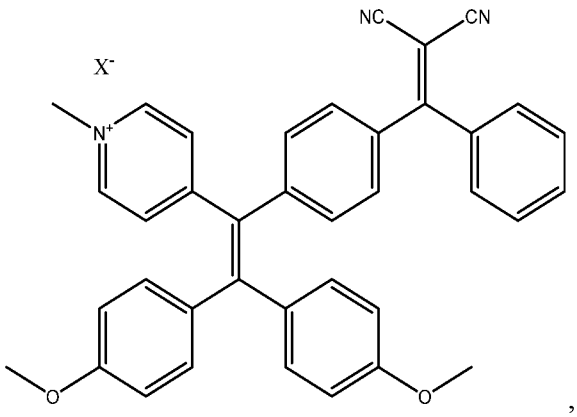

(TPPCN)

,

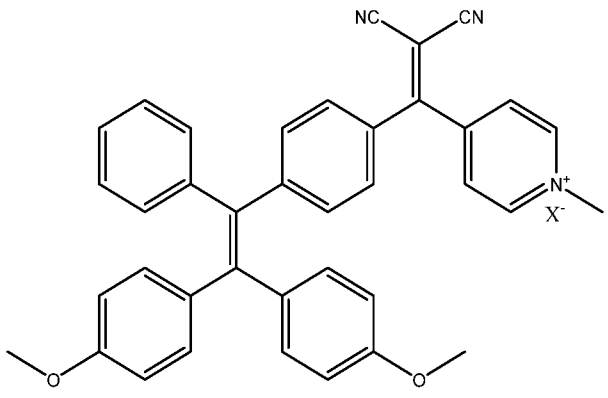

(TPE-CP)

wherein X is selected from the group consisting of I^- and PF_6^-.

BRIEF DESCRIPTION OF DRAWINGS

Various embodiments will now be described in detail with reference to the accompanying drawings.

Fig. 1 depicts the UV spectra of TPPCNin DCM.

Fig. 2A depicts the PL spectra of TPPCN in DCM/Hexane solutions with different fractions of hexane (f_{Hexane}, vol%).

Fig. 2B depicts the relative fluorescence intensities (I/I_0) versus the composition of DCM/Hexane mixtures with TPPCN. Insets: Photographs of TPPCN in DCM/Hexane solutions before (0%) and after (99%) aggregation taken under 365 nm UV light irradiation from a hand-held UV lamp. Concentration: 10 μM; λ_{ex}: 440 nm.

Fig. 3 depicts the cell viability of HeLa cells in the presence of different concentrations of TPPCN.

Fig. 4A depicts fluorescence images of HeLa cells co-stained with TPPCN (5 μM) and MitoTracker red FM (MTR, 100 nM) for 10 min (λ_{ex}: 400-440 nm for TPPCN).

Fig. 4B depicts fluorescence images of HeLa cells co-stained with TPPCN (5 μM) and MitoTracker red FM (MTR, 100 nM) for 10 min (λ_{ex}: 510-550 nm for MTR).

Fig. 4C depicts the images of Figs. 4A and 4B merged, Pearson correlation coefficient Rr = 0.983; scale bar: 20 μm.

Fig. 4D depicts bright-field images of HeLa cells.

Fig. 5A depicts the loss in fluorescence of HeLa cells stained with TPPCN and MTR with the number of scans of laser irradiation.

Fig. 5B depicts confocal images of HeLa cells stained with TPPCN (upper panel) and MTR (lower panel) before and after 50 scans of laser irradiation (about 13min) (concentration: 10 μM (TPPCN) and 100nM (MTR); λ_{ex}:405 nm (TPPCN) and 560 nm (MTR); laser power: 6 μW (TPPCN), 2.16 μW (MTR); scale bar: 20 μm).

Fig. 6depicts the release of ROS monitored by H2DCF-DA: change in fluorescent intensity at 525 nm of TPPCN, H2DCF-DA and their mixture in PBS upon white light irradiation for different time (Concentration: 10 μM (TPPCN), 10 μM (Tetracycline) and 5μM (H2DCF-DA)).

Figs. 7Aand 7B depict the release of ROS monitored by H2DCF-DA in merged bright-field and fluorescence images of HeLa cells stained with TPPCN (10 μM) for 10min and

H2DCF-DA(10 μM) for 60min before (7A) and after (7B) exposure to 405 nm laser for 10s. λ_{ex}: 488 nm; scale bar: 20 μm.

Figs. 7C and7D depict the release of ROS monitored by H2DCF-DA in merged bright-field and fluorescence images of HeLa cells stained with H2DCF-DA (10 μM) for 60 min before (7C) and after (7D) exposure to 405 nm laser for 10 s. λ_{ex}: 488 nm; scale bar: 20 μm.

Figs. 8A and 8Bdepictchange in mitochondrial morphology before and after 10s light irradiation after incubation without TPPCN (10μM) staining for 10min. λ_{ex}: 400-440 nm; scale bar: 15 μm.

Figs. 8C and 8D depict change in mitochondrial morphology before and after 10s light irradiation after incubation with TPPCN (10μM) staining for 10min. λ_{ex}: 400-440 nm; scale bar: 15 μm.

Fig. 9A depicts a confocal image of co-cultured HeLa and MDCK-II cells stained with TPPCN (10 μM).

Fig. 9B depicts a confocal image of co-cultured HeLa and MDCK-II cells stained with TPPCN (10 μM) and H2DCF-DA (10μM) before laser irradiation for 10 s (405 nm); λ_{ex}: 405 nm for TPPCN, 488 nm for H2DCF-DA; scale bar: 20 μm.

Fig. 9Cdepicts a confocal image of co-cultured HeLa and MDCK-II cells stained with TPPCN (10 μM) and H2DCF-DA (10μM) after laser irradiation for 10 s (405 nm); λ_{ex}: 405 nm for TPPCN, 488 nm for H2DCF-DA; scale bar: 20 μm

Fig. 10A depicts a merged bright-field and confocal image of HeLa and MDCK-II cells stained with H2DCF-DA (10 μM) for 60 min before exposure to 405 nm laser for 10 s. λ_{ex} : 488 nm; scale bar: 20 μm.

Fig. 10B depicts a merged bright-field and confocal image of HeLa and MDCK-II cells stained with H2DCF-DA (10 μM) for 60 min after exposure to 405 nm laser for 10 s. λ_{ex} : 488 nm; scale bar: 20 μm.

Fig. 11A depicts a graph of cell viability of HeLa cells in the presence of different concentrations of TPPCN without and with white light irradiation (36mW).

Fig. 11B depicts a graph of cell viability of MDCK-II cells in the presence of different concentrations of TPPCN without and with white light irradiation (36mW).

Fig. 12A depicts a fluorescent image of co-cultured HeLa and MDCK-II cells stained

with TPPCN (10μM) for 40min; then irradiated for 30min under white light (36mW), and then incubated for 24h in dark; and then co-stained with propidium iodide (PI) (1.5 μM) for 15min; λ_{ex}: 400-440 nm for TPPCN; scale bar: 15 μm.

Fig. 12B depicts a fluorescent image of co-cultured HeLa and MDCK-II cells stained with TPPCN (10μM) for 40min; then irradiated for 30min under white light (36mW), incubated for 24h in dark and then co-stained with propidium iodide (PI) (1.5 μM) for 15min; λ_{ex}: 510-540 nm for PI; scale bar: 15 μm.

Fig. 12C depicts a merged fluorescent image of the images of Figs. 12A-12B.

Fig. 12D depicts a bright-field image of the co-cultured HeLa and MDCK-II cells of Figs 12A-12C.

Fig. 12E depicts a fluorescent image of co-cultured HeLa and MDCK-II cells stained without TPPCN (10μM) for 40min; then irradiated for 30min under white light (36mW), incubated for 24h in dark; and then co-stained with propidium iodide (PI) (1.5 μM) for 15min; λ_{ex}: 400-440 nm for TPPCN; scale bar: 15 μm.

Fig. 12F depicts a fluorescent image of co-cultured HeLa and MDCK-II cells stained without TPPCN (10μM) for 40min; then irradiated for 30min under white light (36mW), incubated for 24h in dark and then co-stained with propidium iodide (PI) (1.5 μM) for 15min; λ_{ex}: 510-540 nm for PI; scale bar: 15 μm.

Fig. 12G depicts a merged fluorescent image of the images of Figs. 12E-12F.

Fig. 12H depicts a bright-field image of the co-cultured HeLa and MDCK-II cells of Figs 12E-12G.

Fig. 13A depicts a confocal image of U87 cells co-stained with TPPCN (5μM)and MitoTracker red FM (MTR, 100 nM) for 10 min;λ_{ex}: 405 nm (TPPCN).

Fig. 13B depicts a confocal image of U87 cells co-stained with TPPCN (5μM) and MitoTracker red FM (MTR, 100 nM) for 10 min; λ_{ex}: 561 nm (MTR).

Fig. 13C depicts a merged confocal image of Figs. 13A and 13B.Pearson correlation coefficient Rr = 0.773. Scale bar: 20 μm.

Fig. 13D depicts a graph of cell viabilities of U87 cells in the presence of different concentrations of TPPCN without and with white light irradiation (36mW).

Fig. 14A depicts a merged bright-field and fluorescence image of U87 cells stained with

TPPCN (20 μM,10 min) and H2DCF-DA (10 μM,60 min) before exposure to 405 nm laser for 10 s. λ_{ex}: 488 nm; scale bar: 20 μm.

Fig. 14B depicts a merged bright-field and fluorescence image of U87 cells stained with TPPCN (20 μM,10 min) and H2DCF-DA (10 μM,60 min) after exposure to 405 nm laser for 10 s. λ_{ex}: 488 nm; scale bar: 20 μm.

Fig. 14C depicts a merged bright-field and fluorescence image of U87 cells stained with H2DCF-DA (10μM) for 60 min before exposure to 405 nm laser for 10 s. λ_{ex}: 488 nm; scale bar: 20 μm.

Fig. 14D depicts a merged bright-field and fluorescence image of U87 cells stained with H2DCF-DA (10μM) for 60 min after exposure to 405 nm laser for 10 s. λ_{ex}: 488 nm; scale bar: 20 μm.

Fig. 15A depicts a confocal image of *S. epidermidis* (Gram-positive) incubated with 10μM TPPCN for 10 min. λ_{ex}: 405 nm; scale bar: 10 μm.

Fig. 15B depicts a bright field image of *S. epidermidis* (Gram-positive) incubated with 10 10 μM TPPCN for 10 min. λ_{ex}: 405 nm; scale bar: 10 μm.

Fig. 15C depicts a confocal image of *E.coli* (Gram-negative) incubated with 10 10 μM TPPCN for 10 min. λ_{ex}: 405 nm; scale bar: 10 μm.

Fig. 15D depicts a bright field image of *E.coli* (Gram-negative) incubated with 10 10 μM TPPCN for 10 min. λ_{ex}: 405 nm; scale bar: 10 μm.

Fig. 15E depicts a confocal image of a mixture of *S. epidermidis* (Gram-positive) and *E.coli* (Gram-negative) incubated with 10 10 μM TPPCN for 10 min. λ_{ex}: 405 nm; scale bar: 10 μm.

Fig. 15F depicts a bright field image of a mixture of *S. epidermidis* (Gram-positive) and *E.coli* (Gram-negative) incubated with 10 10 μM TPPCN for 10 min. λ_{ex}: 405 nm; scale bar: 10 μm.

Fig. 16A depicts a bright field image of *S. epidermidis* incubated without 10 μM TPPCN for 10 min followed by white light exposure for 20 min, and stained with 1.5 μM PI for 15

min.(λ_{ex}: 510-550 nm; Scale bar: 15 μm).

Fig. 16B depicts a fluorescent image of *S. epidermidis* incubated B without 10 μM TPPCN for 10 min followed by white light exposure for 20 min, and stained with 1.5 μM PI for 15 min. (λ_{ex}: 510-550 nm; Scale bar: 15 μm).

Fig. 16C depicts a SEM image of *S. epidermidis* incubated without 10 μM TPPCN for 10 min. and then exposed to room light for 1 h (Scale bar: 500 nm).

Fig. 16D depicts a bright field image of *S. epidermidis* incubated with 10 μM TPPCN for 10 min followed by white light exposure for 20 min, and stained with 1.5 μM PI for 15 min.(λ_{ex}: 510-550 nm; Scale bar: 15 μm).

Fig. 16Edepicts a fluorescent image of *S. epidermidis* incubated with 10 μM TPPCN for 10 min followed by white light exposure for 20 min, and stained with 1.5 μM PI for 15 min. (λ_{ex}: 510-550 nm; Scale bar: 15 μm).

Fig. 16F depicts a SEM image of *S. epidermidis* incubated with 10 μM TPPCN for 10 min. and then exposed to room light for 1 h (Scale bar: 500 nm).

Fig. 17A depicts a bright- field image of *E. coli* incubated without 10 μM TPPCN for 10 min followed by white light exposure for 20 min, and stained with 1.5 μM PI for 15 min. (λ_{ex}: 510-550 nm; scale bar: 15 μm).

Fig. 17B depicts a fluorescent image of *E. coli* incubated without 10 μM TPPCN for 10 min followed by white light exposure for 20 min, and stained with 1.5 μM PI for 15 min. (λ_{ex}: 510-550 nm; scale bar: 15 μm).

Fig. 17C depicts a bright- field image of *E. coli* incubated with 10 μM TPPCN for 10 min followed by white light exposure for 20 min, and stained with 1.5 μM PI for 15 min. (λ_{ex}: 510-550 nm; scale bar: 15 μm).

Fig. 17D depicts a fluorescent image of *E. coli* incubated with 10 μM TPPCN for 10 min followed by white light exposure for 20 min, and stained with 1.5 μM PI for 15 min. (λ_{ex}: 510-550 nm; scale bar: 15 μm).

Fig. 18A depicts a bright field image of a mixture of *S. epidermidis* and *E. coli* incubated without 10 μM TPPCN for 10 min followed by white light exposure for 20 min, and staining with 1.5 μM PI for 15 min. (λ_{ex}: 510-550 nm; scale bar: 30 μm).

Fig. 18B depicts a fluorescent image of a mixture of *S. epidermidis* and *E. coli* incubated without 10 μM TPPCN for 10 min followed by white light exposure for 20 min, and staining with 1.5 μM PI for 15 min. (λ_{ex}: 510-550 nm; scale bar: 30 μm).

Fig. 18C depicts a bright field image of a mixture of *S. epidermidis* and *E. coli* incubated with 10 μM TPPCN for 10 min followed by white light exposure for 20 min, and staining with 1.5 μM PI for 15 min. (λ_{ex}: 510-550 nm; scale bar: 30 μm).

Fig. 18D depicts a fluorescent image of a mixture of *S. epidermidis* and *E. coli* incubated with10 μM TPPCN for 10 min followed by white light exposure for 20 min, and staining with 1.5 μM PI for 15 min. (λ_{ex}: 510-550 nm; scale bar: 30 μm).

Figs. 19A and 19B depict graphs of the optical density change of *S. epidermidis* incubated alone, with DMSO, and with TPPCN for different incubation times (Concentration: 10μM TPPCN; 1‰ DMSO).

Figs. 20A and 20B depict graphs of optical density change of *S. epidermidis* incubated in different concentrations of TPPCN for different incubation times.

Figs. 20C and 20D depict graphs of the killing efficiency of different concentrations of TPPCN on *S. epidermidis* at 4h. in 1‰ DMSO.

Fig. 21A depicts plates of *S. epidermidis* without light irradiation (36 mW) for 0.5 h in the absence of TPPCN.

Fig. 21B depicts plates of *S. epidermidis* with light irradiation (36 mW) for 0.5 h in the absence of TPPCN.

Fig. 21C depicts plates of *S. epidermidis*treated with 10 μM TPPCN for 10 min, followed by irradiation with white light (36 mW) for 0.5 h.

Fig. 21D depicts plates *E.coli* without light irradiation (36 mW) for 0.5 h in the absence of TPPCN.

Fig. 21E depicts plates *E.coli* with light irradiation (36 mW) for 0.5 h in the absence of TPPCN.

Fig. 21F depicts plates of *E.coli*treated with 10 μM TPPCN for 10 min, followed by irradiation with white light (36 mW) for 0.5 h.

Fig. 22A depicts plates of *S. epidermidis* without 10 μM TPPCN staining for 30min in the absence of light irradiation.

Fig. 22B depicts plates of *S. epidermidis* with 10 μM TPPCN staining for 30min in the absence of light irradiation.

Fig. 22C depicts plates of *S. epidermidis* treated with 10 μM TPPCN for 30 min, followed by irradiation with white light (36 mW) for 0.5 h.

Fig. 22D depicts plates of *E.coli* without 10 μM TPPCN staining for 30min in the absence of light irradiation.

Fig. 22E depicts plates of *E.coli* with 10 μM TPPCN staining for 30min in the absence of light irradiation.

Fig. 22F depicts plates of *E.coli* treated with 10 μM TPPCN for 30 min, followed by irradiation with white light (36 mW)for 0.5 h.

Fig. 23A depicts a confocal image of a mixture of *S. epidermidis,* HeLa and MDCK-II cells incubated with 10 μM TPPCN for 10 min. (λ_{ex}: 405 nm; scale bar: 15 μm).

Fig. 23B depicts a bright field image of a mixture of *S. epidermidis,* HeLa and MDCK-II cells incubated with 10 μM TPPCN for 10 min. (λ_{ex}: 405 nm; scale bar: 15 μm).

Fig. 23C depicts a merged confocal and bright field image of a mixture of *S. epidermidis,* HeLa and MDCK-II cells incubated with 10 μM TPPCN for 10 min. (λ_{ex}: 405 nm; scale bar: 15 μm).

Fig. 24A depicts a fluorescent image of a mixture of *S. epidermidis* and HeLa cells incubated with 10 μM TPPCN for 10 min followed by white light exposure for 60 min, and staining with 1.5 μM PI for 15 min. (λ_{ex}: 400-440 nm for TPPCN; scale bar: 15 μm).

Fig. 24B depicts a fluorescent image of a mixture of *S. epidermidis* and HeLa cells incubated with 10 μM TPPCN for 10 min followed by white light exposure for 60 min, and staining with 1.5 μM PI for 15 min. (λ_{ex}: 510-540 nm for PI; scale bar: 15 μm).

Fig. 24C depicts a bright-field image of a mixture of *S. epidermidis* and HeLa cells incubated with 10 μM TPPCN for 10 min followed by white light exposure for 60 min, and staining with 1.5 μM PI for 15 min. (λ_{ex}: 400-440 nm for TPPCN, 510-540 nm for PI; scale bar: 15 μm).

Fig. 25 depicts the UV/Vis spectra of TPE-CP in DCM.

Fig. 26A depicts a graph of the PL spectra of TPE-CP in DCM/Hexane solutions with different fractions of hexane (f_{Hexane}, vol%)(Concentration: 10 μM; λ_{ex}: 475 nm).

Fig. 26B depicts a graph of the relative fluorescence intensities (I/I_0) versus the concentration of DCM/Hexane mixtures of TPE-CP(Concentration: 10 μM; λ_{ex}: 475 nm).

Fig. 27 depicts a graph of cell viability of HeLa cells in the presence of different concentrations of TPE-CP.

Fig. 28A depicts a confocal image of HeLa cells co-stained with TPE-CP (10 μM) for 30 min and BODIPY 493/503 (1 μg/ml) for 15 min (λ_{ex}: 488nm for TPE-CP).

Fig. 28B depicts a confocal image of HeLa cells co-stained with TPE-CP (10 μM) for 30 min and BODIPY 493/503 (1 μg/ml) for 15 min (λ_{ex}: 488nm for BODIPY 493/503).

Fig. 28C depicts a merged image of Figs. 28A and 28B, Pearson correlation coefficient Rr = 0.94; Scale bar: 20 μm.

Fig. 29A depicts a graph of loss in fluorescence of HeLa cells stained with TPE-CP and BODIPY 493/503 with the number of scans of laser irradiation.

Fig. 29B depicts confocal images of HeLa cells stained with TPE-CP (upper panels) and BODIPY 493/503 (lower panels), before (left panels) and after (right panels) 50 scans of laser irradiation (about 13 min) (concentration: 20 μM (TPE-CP) and 1μg/mL (BODIPY 493/503); Excitation wavelength :489 nm (TPE-CP) and 489 nm (BODIPY 493/503); laser power: 0.55 μW; scale bar: 20 μm).

Fig. 30A depicts a graph of the release of ROS monitored by H2DCF-DA as measured by the change in fluorescent intensity at 525 nm of TPE-CP, H2DCF-DA and their mixture in PBS

upon white light irradiation for different times (concentration: 10 μM (TPE-CP); 10 μM(Tetracycline), 5μM (H2DCF-DA)).

Fig. 30B depicts a merged bright-field and fluorescent image of HeLa cells stained with TPE-CP (10 μM,30 min) and H2DCF-DA(10 μM,60 min) for 60 min before exposure to 405 nm laser for 30 s. (λ_{ex}: 488 nm; scale bar: 20 μm).

Fig. 30C depicts a merged bright-field and fluorescent image of HeLa cells stained with TPE-CP (10 μM,30 min) and H2DCF-DA(10 μM,60 min)for 60 min after exposure to 405 nm laser for 30 s. (λ_{ex}: 488 nm; scale bar: 20 μm).

Fig. 30D depicts a merged bright-field and fluorescent image of HeLa cells stained with H2DCF-DA (10μM) for 60 min before exposure to 405 nm laser for 30 s. (λ_{ex}: 488 nm; scale bar: 20 μm).

Fig. 30E depicts a merged bright-field and fluorescent image of HeLa cells stained with H2DCF-DA (10μM) for 60 min after exposure to 405 nm laser for 30 s. (λ_{ex}: 488 nm; scale bar: 20 μm).

Fig. 31A depicts a bright field image of *E. coli* (Gram-negative) incubated with 10 μM TPE-CP for 30 min. (λ_{ex}: 400 nm-440 nm; scale bar: 15 μm).

Fig. 31B depicts a fluorescent image of *E. coli* (Gram-negative) incubated with 10 μM TPE-CP for 30 min. (λ_{ex}: 400 nm-440 nm; scale bar: 15 μm).

Fig. 31C depicts a bright field image of *S. epidermidis* (Gram-positive) incubated with 10 μM TPE-CP for 30 min. (λ_{ex}: 400 nm-440 nm; scale bar: 15 μm).

Fig. 31D depicts a fluorescent image of *S. epidermidis* (Gram-positive) incubated with 10 μM TPE-CP for 30 min. (λ_{ex}: 400 nm-440 nm; scale bar: 15 μm).

Figs. 32A and 32B depict optical density changes of *S. epidermidis* incubated alone, with DMSO, and with TPE-CP for different incubation times.(Concentration: 10 μM. 1‰ DMSO).

Fig. 33A depicts a graph of the optical density change of *S. epidermidis* incubated with different concentrations of TPE-CP for different incubation times.(1‰ DMSO).

Fig. 33B depicts a graph of the optical density change of *S. epidermidis* incubated with different concentrations of TPE-CP for different incubation times.(1‰ DMSO).

Fig. 33C depicts a graph of the killing efficiency of different concentrations of TPE-CP on *S. epidermidis* at 4h. (1‰ DMSO).

Fig. 33D depicts a graph of the killing efficiency of different concentrations of TPE-CP on *S. epidermidis* at 4h. (1‰ DMSO).

Fig. 34A depicts images of plates of *S. epidermidis* without light irradiation (36 mW) for 0.5 h in the absence of TPPCN.

Fig. 34B depicts images of plates of *S. epidermidis* with light irradiation (36 mW) for 0.5 h in the absence of TPPCN.

Fig. 34C depicts images of plates of *S. epidermidis* treated with 10 μM TPE-CP for 30 min, without white light irradiation.

Fig. 34D depicts images of plates of *S. epidermidis* treated with 10 μM TPE-CP for 30 min, followed by irradiation with white light (36 mW) for 0.5 h.

Fig. 34E depicts images of plates of *E.coli* without light irradiation (36 mW) for 0.5 h in the absence of TPPCN.

Fig. 34F depicts images of plates of *E.coli* with light irradiation (36 mW) for 0.5 h in the absence of TPPCN.

Fig. 34G depicts images of plates of *E.coli* treated with 10 μM TPE-CP for 30 min, without irradiation with white light (36 mW).

Fig. 34H depicts images of plates of *E.coli* treated with 10 μM TPE-CP for 30 min, followed by irradiation with white light (36 mW)for 0.5 h.

Fig. 35A depicts SEM images of *S. epidermidis* incubated without 10 μM TPE-CP for 10 min, and then exposed to room light for 1 h.

Fig. 35B depicts SEM images of *S. epidermidis* incubated with 10 μM TPE-CP for 10 min, and then exposed to room light for 1 h.

DETAILED DESCRIPTION

The following definitions are provided for the purpose of understanding the present subject matter and for construing the appended patent claims.

Definitions

It should be understood that the drawings described above or below are for illustration purposes only. The drawings are not necessarily to scale, with emphasis generally being placed upon illustrating the principles of the present teachings. The drawings are not intended to limit

the scope of the present teachings in any way.

Throughout the application, where compositions are described as having, including, or comprising specific components, or where processes are described as having, including, or comprising specific process steps, it is contemplated that compositions of the present teachings can also consist essentially of, or consist of, the recited components, and that the processes of the present teachings can also consist essentially of, or consist of, the recited process steps.

In the application, where an element or component is said to be included in and/or selected from a list of recited elements or components, it should be understood that the element or component can be any one of the recited elements or components, or the element or component can be selected from a group consisting of two or more of the recited elements or components. Further, it should be understood that elements and/or features of a composition, an apparatus, or a method described herein can be combined in a variety of ways without departing from the spirit and scope of the present teachings, whether explicit or implicit herein

The use of the terms "include," "includes", "including," "have," "has," or "having" should be generally understood as open-ended and non-limiting unless specifically stated otherwise.

The use of the singular herein includes the plural (and vice versa) unless specifically stated otherwise. In addition, where the use of the term "about" is before a quantitative value, the present teachings also include the specific quantitative value itself, unless pecifically stated otherwise. As used herein, the term "about" refers to a ±10% variation from the nominal value unless otherwise indicated or inferred.

It should be understood that the order of steps or order for performing certain actions is immaterial so long as the present teachings remain operable. Moreover, two or more steps or actions may be conducted simultaneously.

As used herein, "heteroaryl" refers to an aromatic monocyclic ring system containing at least one ring heteroatom selected from oxygen (O), nitrogen (N), sulfur (S), silicon (Si), and selenium (Se) or a polycyclic ring system where at least one of the rings present in the ring system is aromatic and contains at least one ring heteroatom. Polycyclic heteroaryl groups include two or more heteroaryl rings fused together and monocyclic heteroaryl rings fused to one or more aromatic carbocyclic rings, non-aromatic carbocyclic rings, and/or non-aromatic cycloheteroalkyl rings. A heteroaryl group, as a whole, can have, for example, 5 to 22 ring atoms and contain 1 -5 ring heteroatoms (i.e., 5-20 membered heteroaryl group). The heteroaryl group

can be attached to the defined chemical structure at any heteroatom or carbon atom that results in a stable structure. Generally, heteroaryl rings do not contain O—O, S—S, or S—O bonds. However, one or more N or S atoms in a heteroaryl group can be oxidized (e.g., pyridine N-oxide, thiophene S-oxide, thiophene S,S-dioxide). Examples of heteroaryl groups include, for example, the 5- or 6-membered monocyclic and 5-6 bicyclic ring systems shown below:

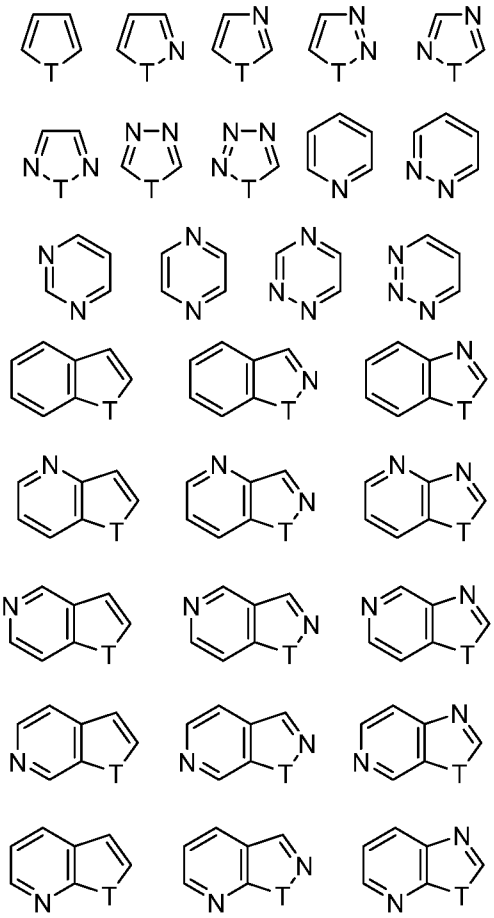

where T is O, S, NH, N-alkyl, N-aryl, N-(arylalkyl) (e.g., N-benzyl), SiH_2, SiH(alkyl), $Si(alkyl)_2$, SiH(arylalkyl), $Si(arylalkyl)_2$, or Si(alkyl)(arylalkyl). Examples of such heteroaryl rings include pyrrolyl, furyl, thienyl, pyridyl, pyrimidyl, pyridazinyl, pyrazinyl, triazolyl, tetrazolyl, pyrazolyl, imidazolyl, isothiazolyl, thiazolyl, thiadiazolyl, isoxazolyl, oxazolyl, oxadiazolyl, indolyl, isoindolyl, benzofuryl, benzothienyl, quinolyl, 2-methylquinolyl, isoquinolyl, quinox-alyl, quinazolyl, benzotriazolyl, benzimidazolyl, benzothiazolyl, benzisothiazolyl, benzisoxazolyl, benzoxadiazolyl, benzoxazolyl, cinnolinyl, lH-indazolyl, 2H-indazolyl, indolizinyl, isobenzofuyl, naphthyridinyl, phthalazinyl, pteridinyl, purinyl, oxazolopyridinyl, thiazolopyridinyl,

imidazopyridinyl, furopyridinyl, thienopyridinyl, pyridopyrimidinyl, pyridopyrazinyl, pyridopyridazinyl, thienothiazolyl, thienoxazolyl, thienoimidazolyl groups, and the like. Further examples of heteroaryl groups include 4,5,6,7-tetrahydroindolyl, tetrahydroquinolinyl, benzothienopyridinyl, benzofuropyridinyl groups, and the like. In some embodiments, heteroaryl groups can be substituted as described herein.

As used herein, "halo" or "halogen" refers to fluoro, chloro, bromo, and iodo.

As used herein, "alkyl" refers to a straight-chain or branched saturated hydrocarbon group. Examples of alkyl groups include methyl (Me), ethyl (Et), propyl (e.g., n-propyl andz'-propyl), butyl (e.g., n-butyl, z'-butyl, sec-butyl, *tert-butyl),* pentyl groups (e.g., n-pentyl,z'-pentyl, -pentyl), hexyl groups, and the like. In various embodiments, an alkyl group can have 1 to 40 carbon atoms (i.e., C1-40 alkyl group), for example, 1-30 carbon atoms (i.e., C1-30 alkyl group). In some embodiments, an alkyl group can have 1 to 6 carbon atoms, and can be referred to as a "lower alkyl group." Examples of lower alkyl groups include methyl,ethyl, propyl (e.g., n-propyl and z'-propyl), and butyl groups (e.g., n-butyl, z'-butyl, *sec-butyl, tert-butyl).* In some embodiments, alkyl groups can be substituted as described herein. An alkyl group is generally not substituted with another alkyl group, an alkenyl group, or analkynyl group.

As used herein, "alkenyl" refers to a straight-chain or branched alkyl group having one or more carbon-carbon double bonds. Examples of alkenyl groups include ethenyl, propenyl, butenyl, pentenyl, hexenyl, butadienyl, pentadienyl, hexadienyl groups, and the like. The one or more carbon-carbon double bonds can be internal (such as in 2-butene) or terminal (such as in 1-butene). In various embodiments, an alkenyl group can have 2 to 40carbon atoms (i.e., C2-40 alkenyl group), for example, 2 to 20 carbon atoms (i.e., C2-20 alkenyl group). In some embodiments, alkenyl groups can be substituted as described herein. Analkenyl group is generally not substituted with another alkenyl group, an alkyl group, or analkynyl group.

As used herein, a "fused ring" or a "fused ring moiety" refers to a polycyclic ring system having at least two rings where at least one of the rings is aromatic and such aromaticring (carbocyclic or heterocyclic) has a bond in common with at least one other ring that canbe aromatic or non-aromatic, and carbocyclic or heterocyclic. These polycyclic ring systems can be highly p-conjugated and optionally substituted as described herein.

As used herein, "heteroatom" refers to an atom of any element other than carbon or hydrogen and includes, for example, nitrogen, oxygen, silicon, sulfur, phosphorus, and selenium.

As used herein, "aryl" refers to an aromatic monocyclic hydrocarbon ring system or a polycyclic ring system in which two or more aromatic hydrocarbon rings are fused (i.e., having a bond in common with) together or at least one aromatic monocyclic hydrocarbon ring is fused to one or more cycloalkyl and/or cycloheteroalkyl rings. An aryl group can have 6 to 24 carbon atoms in its ring system (e.g., C6-24 aryl group), which can include multiple fused rings. In some embodiments, a polycyclic aryl group can have 8 to 24 carbonatoms. Any suitable ring position of the aryl group can be covalently linked to the defined chemical structure. Examples of aryl groups having only aromatic carbocyclic ring(s)include phenyl, 1-naphthyl (bicyclic), 2-naphthyl (bicyclic), anthracenyl (tricyclic), phenanthrenyl (tricyclic), pentacenyl (pentacyclic), and like groups. Examples of polycyclic ring systems in which at least one aromatic carbocyclic ring is fused to one or more cycloalkyl and/or cycloheteroalkyl rings include, among others, benzo derivatives of cyclopentane (i.e., an indanyl group, which is a 5,6-bicyclic cycloalkyl/aromatic ring system), cyclohexane (i.e., a tetrahydronaphthyl group, which is a 6,6-bicycliccycloalkyl/aromatic ring system), imidazoline (i.e., a benzimidazolinyl group, which is a 5,6-bicyclic cycloheteroalkyl/aromatic ring system), and pyran (i.e., a chromenyl group, which is a 6,6-bicyclic cycloheteroalkyl/aromatic ring system). Other examples of aryl groups include benzodioxanyl, benzodioxolyl, chromanyl, indolinyl groups, and the like. In some embodiments, aryl groups can be substituted as described herein. In some embodiments, anaryl group can have one or more halogen substituents, and can be referred to as a "haloaryl" group. Perhaloaryl groups, i.e., aryl groups where all of the hydrogen atoms are replaced with halogen atoms *(e.g.,* -C_6F_5), are included within the definition of "haloaryl." In certain embodiments, an aryl group is substituted with another aryl group and can be referred to as a biaryl group. Each of the aryl groups in the biaryl group can be substituted as disclosed herein.

As used herein, a "theranostic agent" refers to an organic material having both diagnostic and therapeutic capabilities.

Unless defined otherwise, all technical and scientific terms used herein have the same meaning as commonly understood to one of ordinary skill in the art to which the presently described subject matter pertains.

Where a range of values is provided, for example, concentration ranges, percentage ranges, or ratio ranges, it is understood that each intervening value, to the tenth of the unit of the lower limit, unless the context clearly dictates otherwise, between the upper and lower limit of

that range and any other stated or intervening value in that stated range, is encompassed within the described subject matter. The upper and lower limits of these smaller ranges may independently be included in the smaller ranges, and such embodiments are also encompassed within the described subject matter, subject to any specifically excluded limit in the stated range. Where the stated range includes one or both of the limits, ranges excluding either or both of those included limits are also included in the described subject matter.

Throughout the application, descriptions of various embodiments use "comprising" language. However, it will be understood by one of skill in the art, that in some specific instances, an embodiment can alternatively be described using the language "consisting essentially of" or "consisting of".

For purposes of better understanding the present teachings and in no way limiting the scope of the teachings, unless otherwise indicated, all numbers expressing quantities, percentages or proportions, and other numerical values used in the specification and claims, are to be understood as being modified in all instances by the term "about". Accordingly, unless indicated to the contrary, the numerical parameters set forth in the following specification and attached claims are approximations that may vary depending upon the desired properties sought to be obtained. At the very least, each numerical parameter should at least be construed in light of the number of reported significant digits and by applying ordinary rounding techniques.

Theranostic agents

The present subject matter relates to an AIE luminogen probe that can be used as a theranostic agent. The theranostic agent can be used for the selective imaging and killing of harmful cells. The harmful cells can include cancer cells and Gram-positive bacteria. The theranostic agent can be administered to a patient undergoing a surgical procedure in order to selectively identify and/or kill harmful cells. The theranostic agent may in administered *in situ* at the site of the surgical procedure. The theranostic agent may allow selective imaging of cancer cells and/or gram-positive bacteria through AIE mediated fluorescence. The theranostic agent may be used in photodynamic therapy to kill or impair the growth of the harmful cells by exposure of the theranostic agent to white light.

In an embodiment, the present AIE luminogen probe is a small molecule, organic compound that has a chemical structure selected from the group consisting of:

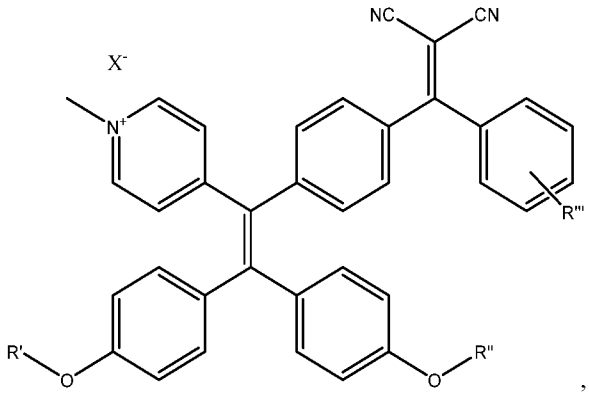
NC
CN
X-
N+
R'''
R'
O
O
R''

,

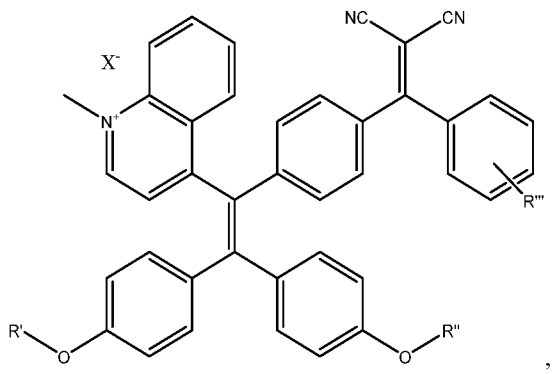
NC
CN
X-
N+
R'''
R'
O
O
R''

,

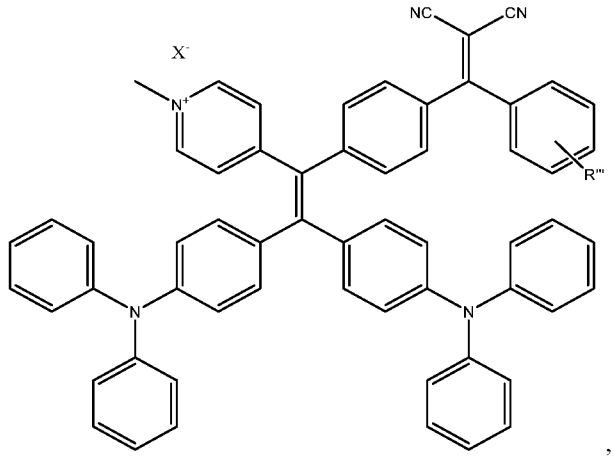
NC
CN
X-
N+
R'''
N
N

,

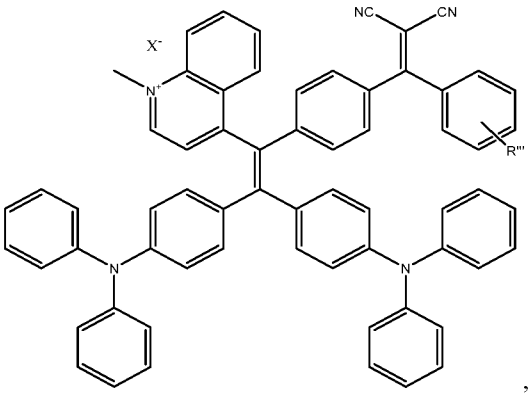
NC
CN
X-
N+
R'''
N
N

,

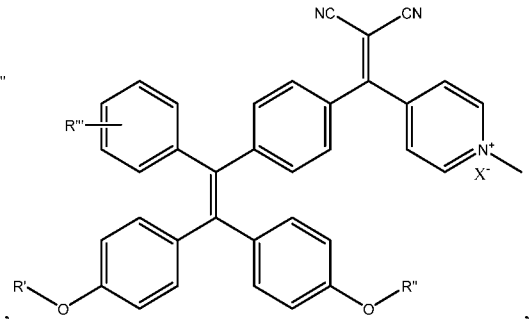
NC
CN
R'''
N+
X-
R'
O
O
R''

,

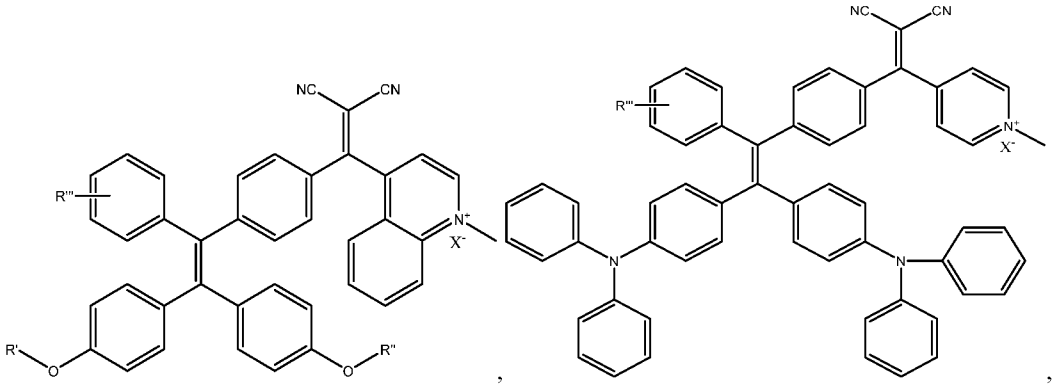

, and

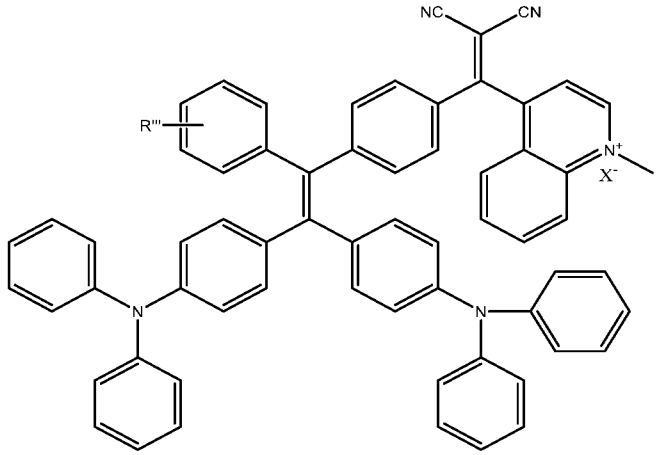

;

wherein R', R", and R"' are independently selected from the group consisting of H, alkyl, unsaturated alkyl, heteroalkyl, cycloalkyl, heterocycloalkyl, aryl, heteroaryl, alkyl-NCS, alkyl-N_3, and alkyl-NH_2; and

wherein the counteranion X^- is selected from the group consisting of I^-, PF_6^-, BF_4^-, SbF_6^-, SbF_5^-, CH_3COO^-, CF_3COO^-, CO_3^{2-}, SO_4^{2-}, SO_3^{2-}, $CF_3SO_2^-$, TsO^-, ClO_4^-, F^-, Cl^-, Br^-, $(F_3CSO_2)N^-$, and PO_4^{3-}.

In a further embodiment, the compound has a chemical structure selected from the group consisting of:

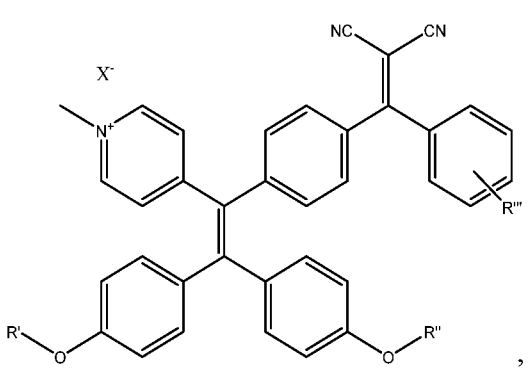

, and

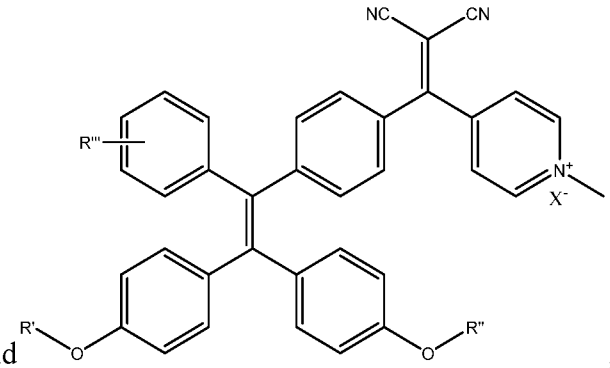

;

wherein R', R", and R"' are independently selected from the group consisting of H, alkyl, unsaturated alkyl, heteroalkyl, cycloalkyl, heterocycloalkyl, aryl, heteroaryl, alkyl-NCS, alkyl-N_3, and alkyl-NH_2; and

wherein the counteranion X^- is selected from the group consisting of I^-, PF_6^-, BF_4^-, and SbF_6^-.

In an embodiment, the compound has one of the following structural formulae:

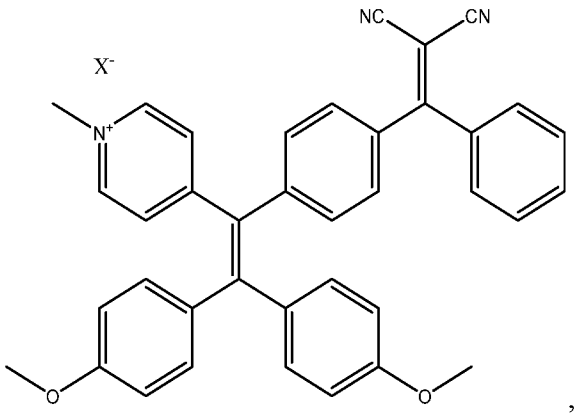

,

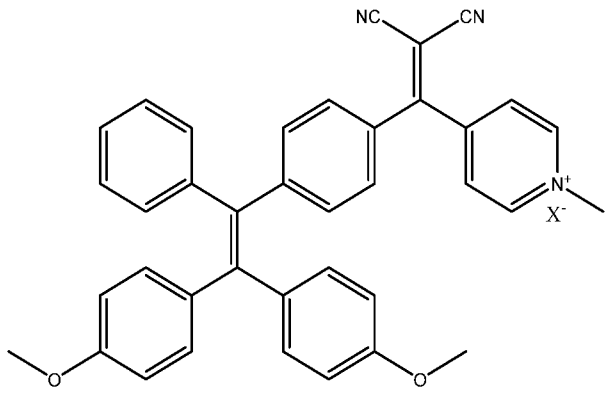

(TPPCN) (TPE-CP)

wherein X is selected from the group consisting of I^- and PF_6^-.

An exemplary reaction scheme for preparing the TPPCN compound is provided below:

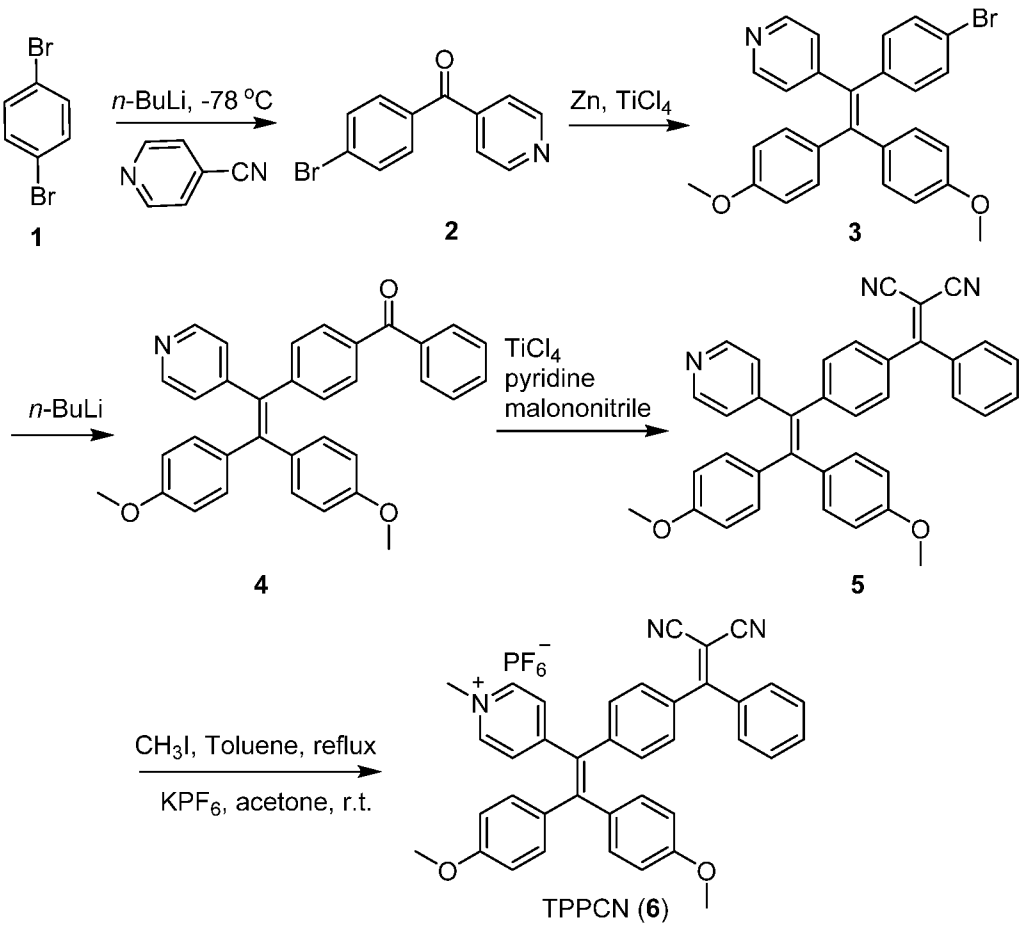

An exemplary reaction scheme for preparing the TPE-CP is provided below:

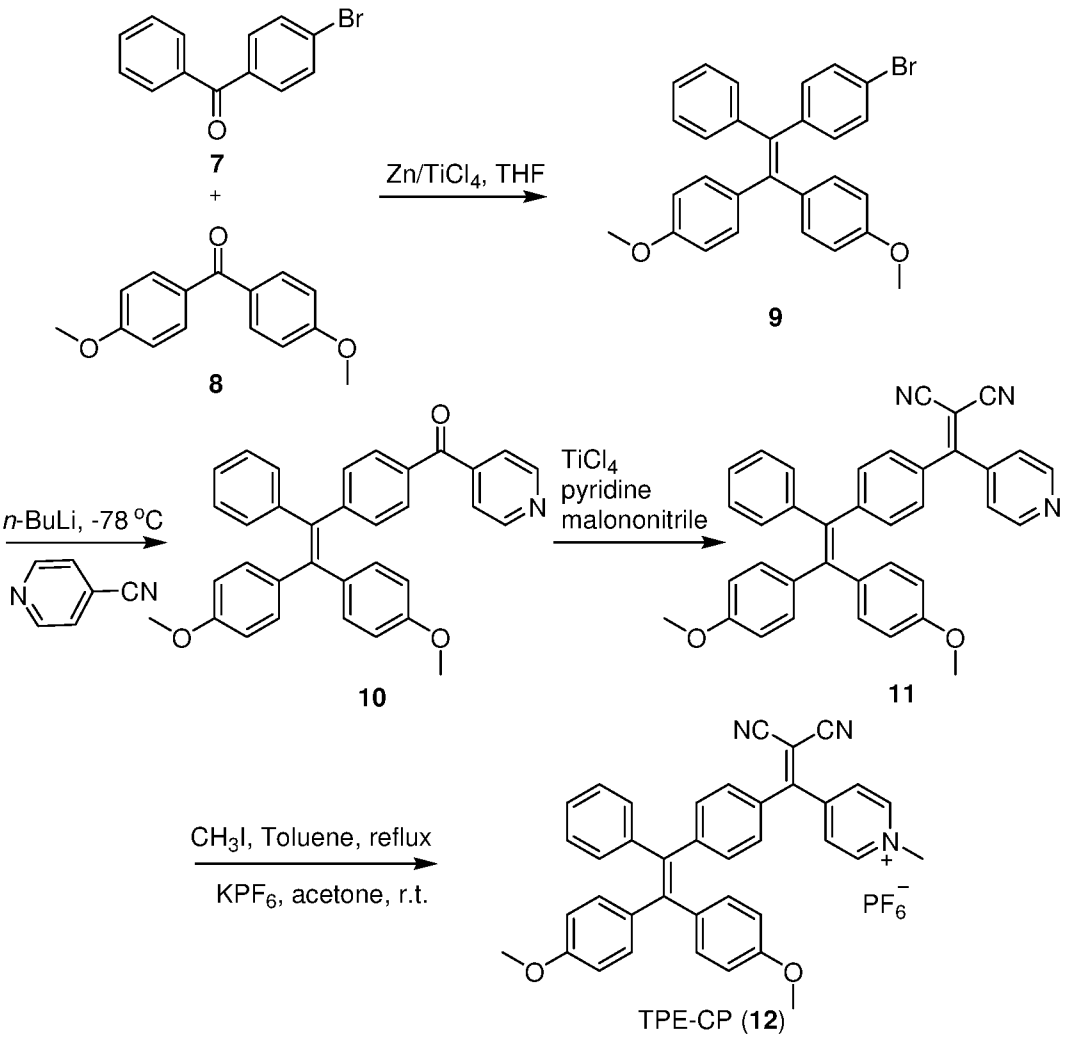

Selectively Identifying Harmful Cells and Stopping Cell Growth

The present compounds can be administered to a patient as a contrast agent for locating harmful cells in the patient using *in vivo* imaging techniques, for example, fluorescent imaging. For patients undergoing a surgical procedure, the compounds can be administered *in situ*, for example. This *in situ* administration may be used to detect the continued presence of cancer cells during a tumor ablation procedure, or to detect the presence of potentially harmful (Gram-positive) bacteria in or near the surgical site. In another embodiment, the compounds can be administered via intravenous injection, for example.

As set forth in detail herein, imaging studies demonstrate that the compounds can serve

as an effective probe to selectively identify cancer cells and gram-positive bacteria. Once harmful cells have been identified, the compounds can be exposed to white light, causing the compounds to act as photosensitizers, resulting in production of reactive oxygen species and selective cytotoxicity to the harmful cells. In an embodiment, the harmful cells may be cancer cells and/or gram-positive bacteria. Photodynamic treatment of harmful cells using these compounds may result in impaired cellular growth or cell death.

As the present compounds are completely organic, these compounds show good biocompatibility, and no detectable side toxicity. The compounds demonstrate ultra-high stability and good photodynamic performance, making them promising candidates for *in situ* diagnosis and therapy applications.

The present teachings are illustrated by the following examples.

EXAMPLES

Materials and Instruments

Minimum essential medium (MEM), Dulbecco's modified eagle medium (DMEM), fetal bovine serum (FBS), penicillin and streptomycin, phosphate buffered saline (PBS), MitoTracker® Red FM and BODIPY 493/503 were purchased from Invitrogen. LB agar and LB broth were purchased from USB Co. Propidium iodide (PI) and H2DCF-DA were purchased from Sigma-Aldrich and used as received. THF were purified by distillation from sodium benzophenone ketyl immediately prior to use. Other reagents used in this work, such as dimethyl sulfoxide, potassium chloride and sodium chloride were purchased from Sigma-Aldrich and used as received without further purification. Milli-Q water was supplied by a Milli-Q Plus System (Millipore Corporation, United States). All the chemicals used in the synthesis of TPPCN and TPE-CP are purchased from Sigma-Aldrich.

Characterization

^{1}H and ^{13}C nuclear magnetic resonance (NMR) spectra were recorded on a Bruker AV 400 spectrometer using CD_2Cl_2as the deuterated solvent. High-resolution mass spectra (HRMS) were measured on a Finnegan MAT TSQ 7000 Mass Spectrometer System in MALDI-TOF mode. The UV absorption spectra were performed on a Milton Ray Spectronic 3000 array spectrophotometer. Steady-state fluorescence spectra were recorded on a Perkin Elmer LS 55 spectrometer. Fluorescence images were collected on an Olympus BX 41 fluorescence

microscope. Laser confocal scanning microscope images were collected on a Zeiss laser scanning confocal microscope (LSM7 DUO) and analyzed using ZEN 2009 software (Carl Zeiss). Particle sizes were measured on a Zeta potential analyzer (Brookhaven, ZETAPLUS). The observation of bacterial morphology was investigated using Scanning Electron Microscopy (JSM-6390 (JEOL)).

Cell Culture

HeLa cells were cultured in the MEM containing 10% FBS and antibiotics (100 units/mL penicillin and 100 g/mL streptomycin) in a 5% CO_2 humidity incubator at 37 °C. MDCK-II and U87 cells were cultured DMEM containing 10% FBS and antibiotics (100 units/mL penicillin and 100 g/mL streptomycin) in a 5% CO_2 humidity incubator at 37 °C.

Biocompatibility

MTT assays were used to evaluate the cytotoxicity of TPPCN and TPE-CP. Cells were seeded in 96-well plates (Costar, IL, USA) at a density of 5×10^3 cells/well. After overnight culturing, media in each well were replaced by 100 μL fresh medium containing different concentrations of TPPCN and TPE-CP. The volume fraction of DMSO was below 0.2%. 24 hours later, 10 μL MTT solution (5mg/mL in PBS) was added into each well. After 4 hours of incubation, 100 μL SDS-HCl aqueous solution (10% SDS and 0.01 M HCl) was added to each well. After incubation for 6 hours, the absorption of each well at 595 nm was recorded via a plate reader (Perkin-Elmer Victor3TM). Each trial was performed with 6 wells in parallel.

Cytotoxicity

HeLa, MDCK-II or U87 cells were seeded in 96-well plates (Costar, IL, USA) at a density of 5×10^3 cells/well. After overnight culturing, media in each well were replaced by 100 μL fresh medium containing different concentrations of TPPCN. The volume fraction of DMSO is below 0.2%. After 8 h incubation, three plates containing HeLa, MDCK-II and U87 cells were exposed to white light (36 mW) for 30 min. and another three plates with cells were kept in dark as control. Then the biocompatibility test was performed on these plates as described above.

Cell Imaging

Cells were grown overnight on a 35 mm petri dish with a coverslip or a plasma-treated 25 mm round cover slip mounted at the bottom of a 35 mm petri dish with an observation window. Live cells were incubated with certain dyes at certain concentrations for certain times (by adding 2 μL of a stock solution in DMSO solution to 2 mL of cell culture medium, DMSO < 0.1 vol%).

The dye-labelled cells were mounted and imaged under a fluorescence microscope (BX41 Microscope). Conditions: for TPPCN and TPE-CP, excitation filter = 400-440 nm, dichroic mirror = 455 nm, and emission filter = 465 nm long pass; for MitoTracker red FM, excitation filter = 510-550 nm, dichroic mirror = 570 nm, and emission filer = 590 nm long pass; for BODIPY, excitation filter = 460-490 nm, dichroic mirror = 505 nm, and emission filer = 515 nm long pass.

Photostability

Dye-labelled HeLa cells were imaged by a confocal microscope (Zeiss laser scanning confocal microscope LSM7 DUO) using ZEN 2009 software (Carl Zeiss). Conditions: for TPPCN, excitation wavelength: 405 nm; for MitoTracker red FM, excitation wavelength: 560 nm; laser powers were unified as 6 μW (TPPCN) and 2.16 μW (MTR). For TPE-CP and BODIPY 493/503, excitation wavelength: 489 nm; laser powers were unified as 0.55 μW.

Bacterial Culturing, Imaging, and Killing

A single colony of bacteria on solid culture medium [Luria broth (LB) for *E. coli* and *S. Epidermidis*] was transferred to 5 mL of liquid culture medium and grown at 37 ^{o}C for 10 h. The concentrations of bacteria were determined by measuring optical density at 600 nm (OD600) and then 1 × 10^{9} colony forming unit (CFU) of bacteria were transferred to a 1.5 mL EP tube. Bacteria were harvested by centrifuging at 13000 rpm for 3 min. After removal of supernatant, 1 mL dye solution in PBS at certain concentration was added into the EP tube. After dispersing with vortex, the bacteria were incubated at room temperature for certain time.

To take fluorescence images, about 2 μL of stained bacteria solution was transferred to a glass slide and then covered by a coverslip. The image was collected using 100 × objectives. The bacteria were imaged under an FL microscope (BX41 Microscope) using different combinations of excitation and emission filters for each dye: for TPPCN and TPE-CP, excitation filter = 400-440 nm, dichroic mirror = 455 nm, and emission filter = 465 nm long pass; for PI, excitation filter = 510-550 nm, dichroic mirror = 570 nm, and emission filter = 590 nm long pass.

For PI staining experiments, after incubation with 10 μM of TPPCN for 10 min, the bacteria were exposed to white light for 20 min, while the control group was put in the dark. Afterwards, PI was added to both the experiment and control groups at a final concentration of 1.5 μM, followed by incubation in the dark for another 15 min. Then the bacteria were imaged under the fluorescent microscope with the following setting: excitation filter = 510-550 nm,

dichroic mirror = 570 nm, and emission filter = 590 nm long pass.

For the light-induced toxicity experiment, 1×10^8 CFU bacteria were dispersed in 1 mL PBS. After incubation with the 10 μM of TPPCN for 10 min or with 10 μM of TPE-CP for 30 min, the solution was centrifuged at 13000 rpm for 3 min, followed by removal of the supernatant and washing with PBS. Then the bacteria were dispersed in PBS and exposed to white light for the designed periods of time, while the control groups were placed in dark. Then the viability of bacteria was evaluated by the plate-count method.

For antibiosis studies, the concentration of microbe was diluted to an optical density at 600 nm (OD600) of nearly 0.2. TPPCN with various predetermined concentrations was added to the individual tubes. The same amount of pure DMSO was also added to the control tube. At the designed time intervals, the concentrations of microbe were determined by measuring OD600. The tests were repeated three times to ensure reliability.

For SEM studies, the concentration of *S. epidermidis* was diluted to an optical density at 600 nm (OD600) of nearly 0.2. The bacteria were incubated with 10μM TPPCN for 4 h and illuminated with white light for 1 h, followed by drying, and collection of SEM images. Bacteria without treatment were also imaged under SEM for comparison.

Example 1

Synthesis of TPPCN and TPE-CP

4-(1-(4-(2,2-dicyano-1-phenylvinyl)phenyl)-2,2-bis(4-methoxyphenyl)vinyl)-1-methylpyridinium hexafluorophosphate (TPPCN, **6**)

$TiCl_4$ (1 mL, 9.0 mmol) was slowly added into a suspension of Zn dust (1.17 g, 18.0 mmol) in dry THF (50 mL) at -78 °C to form a reaction mixture. After reflux for 2 h, a mixture of 4,4'-dimethoxyphenylmethanone (1.090 g, 4.5 mmol) and compound **2** (0.786 g, 3 mmol) in dry THF (20 mL) was added to the reaction mixture. The reaction mixture was refluxed for another 5 h. After removal of the solvent by compressed air, the residue was extracted with DCM and dried over anhydrous Na_2SO_4. The crude product was purified on a silica-gel column using DCM as eluent. Compound **3** was isolated as yellow solid with a 50% yield.

n-BuLi (0.6 mL, 1.2 mmol, 2.0 M in hexane) was added dropwise to a solution of compound **3** (0.471 g, 1.0 mmol) in dry THF (20 mL) at -78 °C under an atmosphere of N_2. After stirring for 2 h at this temperature, *N,N*-dimethylbenzamide (0.179 g, 1.2 mmol) was slowly added to the mixture and stirring was continued at -78 °C for 1 h. The mixture was then allowed

to warm to room temperature (22 °C), quenched with 10% aqueous HCl (10 mL), and stirred for 30 min. The aqueous phase was separated and washed with DCM (3 × 10 mL), dried over anhydrous $MgSO_4$, and evaporated in vacuo. The crude product was subsequently reacted with malonitrile under refluxing in the presence of $TiCl_4$ and pyridine, producing a mixture that was purified on a silica gel column using DCM as eluent to give compound **5** as a light-yellow solid (0.382 g, 70%).

A toluene solution of compound **5** (0.50 mmol) was added to methyl iodide (5 mmol CH_3I) to form a reaction mixture. The reaction mixture was heated and stirred under nitrogen at 110 °C for 4 h. A precipitate was collected and washed with toluene. A crude product was recrystallized using the mixed solvents hexane and dichloridemethane. The pure product was dissolved into acetone and counterion exchanged with potassium hexafluorophosphate to obtain orange-color TPPCN (yield 90%). ^{1}H-NMR (400MHz; CD_2Cl_2) δ H 8.15 (d, 2H), 7.61 (t, 1H), 7.52 (t, 2H), 7.45-7.42 (m, 4H), 7.31 (d, 2H), 7.16 (d, 2H), 7.03(d, 2H), 6.94 (d, 2H), 6.83 (d, 2H), 6.70 (d, 2H), 4.22 (s, 3H), 3.81 (s, 3H), 3.76 (s, 3H) ppm; ^{13}C-NMR (400MHz; CD_2Cl_2) δ C 174.0, 161.4, 161.0, 153.1, 146.0, 143.5, 135.8, 135.4, 133.3, 133.2, 132.7, 132.6, 132.0, 131.5, 130.9, 130.4, 129.7, 128.9, 114.4, 113.9, 113.8, 113.5, 81.7, 55.4, 55.3, 47.7 ppm; MALDI-MS calculated for cation of TPPCN ($C_{38}H_{30}N_3O_2^+$): 560.2333, found: 560.2355.

4-(1-(4-(2,2-bis(4-methoxyphenyl)-1-phenylvinyl)phenyl)-2,2-dicyanovinyl)-1-methylpyridinium hexafluorophosphate (TPE-CP, **12**)

The entire synthesis process of TPE-CP was performed along similar lines to the synthesis of TPPCN discussed above, followed by addition of a toluene solution of compound **11** (0.50 mmol) to methyl iodide (5 mmol CH_3I) to form a reaction mixture. The reaction mixture was heated and stirred under nitrogen at 110 °C for 4 h. A precipitate was collected and washed with toluene. A crude product was recrystallized using the mixed solvents hexane and dichloridemethane. The pure crystallized product was dissolved into acetone and the counterion was exchanged with potassium hexafluorophosphate to obtain dark red-color TPE-CP (yield 90%). ^{1}H-NMR (400MHz; CD_2Cl_2) δ H 8.76 (d, 2H), 7.99 (d, 2H), 7.27 (d, 2H), 7.20-7.14 (m,5H), 7.06-7.03 (m, 2H), 6.95-6.91 (m, 4H), 6.70-6.63 (m, 4H), 4.51 (s, 3H), 3.75 (s, 3H), 3.73 (s, 3H) ppm; ^{13}C-NMR (400MHz; CD_2Cl_2) δ C 171.2, 158.9, 158.6, 152.6, 150.4, 145.9, 145.8, 143.1, 137.7, 137.4, 135.5, 135.4, 132.7, 132.6, 132.5, 132.2, 131.8, 131.4, 131.3, 130.0, 129.9,

129.8, 129.0, 128.0, 127.5, 126.8, 126.6, 113.4, 113.3, 113.2, 113.0, 84.9, 55.1, 55.0, 49.4 ppm; MALDI-MS calculated for cation of TPE-CP ($C_{38}H_{30}N_3O_2^+$): 560.2333, found: 560.2321.

Example 2

Photophysical Properties of TPPCN

The UV-vis absorption spectrum of TPPCN was recorded in DCMsolution, as shown in Fig. 1. TPPCN shows an absorption maximum at 440 nmlocated in the range of visible light, which will cause less damage to biological system than UV light would. TPPCNdisplays the AIE feature, as evidenced by the photoluminescence (PL) spectra recorded in the solution and aggregate states. As shown in Figs. 2A-2B, TPPCN emits faintly in Hexane/DCM mixtures with the hexane fraction from 0 to 70%. When the hexane fraction is increased to 80%, the fluorescence gradually emerged with a peak at 606 nm. Upon further increasing the hexane to 90%, the PL intensity peaked about 217-fold higher than that in found in the pure DCM solution. Bright yellow fluorescence was observed under 365 nm UV illumination from a hand-held UV lamp. Such a distinct emission difference is possibly due to the formation of aggregates of TPPCN induced by hexane as a poor solvent for TPPCN. The PL intensity then decreases when the hexane content increases from 90%-99%, potentially as a result of TPPCN precipitation on the inner wall of the cuvette. These precipitates can be observed by naked eye under UV illumination. The quantum yield (QY) in pure DCM and in the DCM/hexane mixture (1: 99, v/v) was 0% and 15.2%. The PL and QY results demonstrate that TPPCN is AIE-active.

Example 3

Biocompatibility of TPPCN

Cytotoxicity of TPPCNon HeLa cells was determined using the 3-(4,5-dimethyl-2-thiazolyl)-2,5-diphenyltetrazolium bromide (MTT) assay. Cell viability was not significantly affected when the concentration of TPPCN was raised to 10μM (as shown in Fig. 3),indicative of negligible cytotoxicity and good biocompatibility to HeLa cells within the tested concentration range.

Example 4

TPPCN Mitochondrial Targeting

TPPCN's capability to stain mitochondria in HeLa cells was investigated. HeLa cells were co-stained with TPPCN and MitoTracker Red FM (MTR), a commercially available mitochondria imaging agent for 10 min. As demonstrated in Figs. 4A-4D,TPPCN can selectively accumulate in cellular mitochondria and emits strong blue-green fluorescence. Red fluorescence from MTR is observed and merged quite well with blue-green fluorescence. Pearson's correlation coefficient (R_r; from +1 to -1), which is used to evaluate the linear association of two variables, is calculated to be 0.983, suggesting that TPPCN is highly specific to mitochondria.

Example 5

Photostability

As one of the key criteria for evaluating a fluorescent visualizer, the photostability of TPPCN was assessed by sequential scanning with confocal microscope. As shown in Figs. 5A-5B,the fluorescence of TPPCN can still be observed in mitochondria clearly and more than 95% signal is retained after 50 scans of about 13 min. irradiation. By contrast, more than half of the fluorescence of MTR is lost after 25 scans and the red emission of MTR almost disappears after 50 scans. Evidently, TPPCN shows a much higher photostability than MTR.

Example 6

ROS Generation

More interestingly, TPPCN is also a photosensitizer for ROS generation. Since TPPCN absorbs strongly in the visible light region, white light was used as the excitation light source. H2DCF-DA, which emits fluorescence at around 530 nm in the presence of ROS, was used as a ROS indicator. In the presence of TPPCN, the fluorescence of H2DCF-DA is gradually enhanced with the irradiation time increasing (as shown in Fig. 6). After 30 min. white light illumination, the intensity of H2DCF-DA was 500 times higher than the original emission intensity. Such change, however, was not observed in TPPCN or H2DCF-DA alone. Compared with Tetracycline, a commonly used photosensitizer, the ROS generation efficiency of TPPCN is much higher. Furthermore, the ROS generation efficiency of TPPCN inside the cells was then investigated. As shown in Figs.7A-7D, before 405 nm laser irradiation, almost no emission from H2DCF-DAcould be detected in the cells. After 405 nm laser irradiation for 10 s, the green

emission of H2DCF-DA was observed. For the cells incubated with H2DCF-DA alone, the emission remains faint both before and after 405 nm laser irradiation. These results indicate that TPPCN could serve as a sensitizer for ROS generation both in solution and in cells.

Excessive amounts of ROS are detrimental to cells. As depicted in Figs. 8A-8D, the mitochondria morphology of dye-stained HeLa cells changed from long tubular-like, to small and dispersed fragments after 10 s light irradiation. In contrast those treated without TPPCN still keep very well, suggesting that the ROS generated from TPPCN can cause damage to the mitochondria and lead to cell death.

Example 7

Selective Imaging and Killing of Cancer Cells

TPPCN can selectively stain cancer cells over normal cells. Cancerous HeLa cells and normal MDCK-II cells were incubated with TPPCN respectively under the same conditions. As shown in Fig. 9A,strong blue-green fluorescence was observed in the mitochondria of HeLa cells. On the contrary, almost no fluorescence was observed in MDCK-II cells. This result is sufficient to validate the hypothesis that the distinction of MMP between cancer cells and normal cells as well as the electrostatic interaction enable such cancer cells differentiation.

To demonstrate the ability of TPPCN to selectively killing of cancer cells the ROS generation efficiency of TPPCN inside the cells in the co-culture system was investigated. Before 405 nm laser irradiation, almost no emission from the cells could be detected in the cells (Fig. 9B). After 405 nm laser irradiation for 10 s, the green emission of H2DCF-DA was observed in HeLa cells. While almost no fluorescence was observed in MDCK-II cells(Fig. 9C). For the cells incubated with H2DCF-DA alone, the emission remains faint both before and after 405 nm laser irradiation (Fig. 10A-10B). The results indicate that TPPCN could selectively serve as a sensitizer for ROS generation in cancer cells in the co-culture system.

The MTT assay was applied to check the cell viability of HeLa cells and MDCK-II cells. For HeLa cells, in the absence of TPPCN, the white light illumination brings almost no change in the cell viability. However, for those stained with TPPCN, cell viability decreases upon white light irradiation along with the increasing concentration of TPPCN (Fig. 11A). It is worth noting that negligible change in cell viability was observed when TPPCN-stained cells were kept in the

dark without light irradiation. As a comparison, almost no toxicity on MDCK-II cells was found even when the concentration of TPPCN reached to 12.5 μM with light irradiation (Fig. 11B), in which condition the survival rate of HeLa cells, however, decreased by almost 80%.This suggests that the simultaneous combination of TPPCN and light irradiation will cause a therapeutic effect to cancer cells but not to non-cancerous cells, demonstrating good potential of TPPCN as a theranostic system that can selectively target the mitochondria in cancer cells and induce their death by photodynamic therapy.

To further examine the selectively cytotoxicity to cancer cells in the co-culture system, propidium iodide (PI) staining was applied. PI is a cell impermeable dye, which stains dead cells or late apoptotic cells with damaged membrane only. As shown in Figs. 12A-12Honly HeLa cells (not MDCK-II cells) emit blue-green light with TPPCN staining. Upon white light irradiation, red emission from PI was observed in all the HeLa cells stained with TPPCN, indicating that these cells are effectively killed by the TPPCN-sensitized ROS generation. Control groups of unstained cells with white light treatment cannot be stained with PI, proving the vital role of TPPCN in causing the cell death.

Another kind of cancer cell line (U87, commonly used in neuroscience) was used to confirm the universal mitochondria selectivity and killing effect of TPPCN. As demonstrated in Figs. 13A-13D and Figs. 14A-14D, TPPCN can specifically target the mitochondria of U87 cells and can selectively serve as a sensitizer for ROS generation in U87 cells.

Example 8

Selective Imaging and Killing of Gram-Positive Bacteria

Similar to the difference of MMP of cancer cells and normal cells, Gram-positive bacteria have much more negative charge than Gram-negative bacteria due to the teichoic acid found on the Gram-positive bacterial membrane. Therefore, TPPCN was applied to bacterial differentiation imaging. For biosafety nonpathogenic bacteria *S. epidermidis* and *E. coli* were selected as a representative species for this study. As shown in Figs. 15A-15B, after incubation with 10 μM TPPCN for 10 min, Gram-positive bacteria *S. epidermidis* are clearly visualized. The Gram-negative bacteria *E. coli*, however, cannot be observed (Figs. 15C-D), indicating that TPPCN selectively stains Gram-positive bacteria over Gram-negative bacteria. These results

were confirmed in a co-culture system of Gram-positive and Gram-negative bacteria (Figs. 15E-F).

The killing effect of TPPCN on both Gram-positive and Gram-negative bacteria was evaluated with the aid of propidium iodide (PI), which can selectively light up dead bacteria. The bacteria were first incubated with TPPCN for 10 min, and then stained with PIafter being illuminated under white light for 20 min. As shown in Figs. 16A-16F, *S. epidermidis* were incubated without (Figs. 16A-16B), and with (Figs. 16D-16E) 10 μM TPPCN for 10 minutes followed by white light exposure for 20 minutes and staining with 1.5 μM PI for 15 minutes. Almost no red emission from PI can be observed in the control groups (Figs. 16A-16B), while bright red emission from PI can be clearly observed in the TPPCN-stained cells (Figs. 16D-16E). As PI selectively penetrates bacteria with damaged membranes, this confirms that TPPCN can kill *S. epidermidis* under white light irradiation.

The antibacterial effect of TPPCN on *S. epidermidis* was further investigated by scanning electron microscopy (SEM). SEM was used to determine whether bacterial death resulting from exposure to TPPCN and white light irradiation involved destruction of the integrity of bacterial cell walls. In the absence of TPPCN, the morphology of *S. epidermidis* remained regular, bearing the characteristics of clear borders and smooth bodies (Fig. 16C). A well-defined border between overlapping bacteria is clearly resolved, indicating the presence of intact *S. epidermidis* cell walls. Upon treatment with TPPCN and white light irradiation, the cell walls of *S. epidermidis* shrank and split and bacterial shape changed dramatically (Fig. 16F).

As shown in Fig. 17A-17D, *E. coli* were incubated without (Figs. 17A-17B) and with (Figs. 17C-17D) 10 μM TPPCN for 10 minutes, followed by white light irradiation for 20 minutes and staining with 1.5 μM PI for 15 minutes. Almost no red emission from PI is observed, indicating that *E. coli* are not killed by TPPCN under white light irradiation.

Taken in combination, the experiments illustrated in Figs. 16A-16F and 17A-17D demonstrate that TPPCN serves as a photosensitizer to kill *S.epidermidis* upon white light irradiation by causing damage to the cell wall and the killing effect of TPPCN on *E. coli* is less significant than on *S. epidermidis*. Similar results were confirmed in a co-culture system of Gram-positive and Gram-negative bacteria (Figs. 18A-18D). These results also confirm that TPPCN is a good candidate for use in PDT.

The antibiosis capability of TPPCN was further explored. Based on the killing effect on *S. epidermidis*, the optical density (OD600) change of bacteria incubated with the TPPCN was investigated. As illustrated in Figs. 19A-19B, TPPCN exhibits an inhibition effect on the proliferation of *S. epidermidis*. The time-dependent and concentration-dependent OD600 changes of *S. epidermidis* incubated with TPPCN are shown in Figs. 20A-20B. According to the curve plotted by concentration-dependent OD600 changes incubated with TPPCN (Figs. 20C-20D), the IC_{50} of TPPCN for inhibition of *S. epidermidis* growth is estimated to be 3.068 μM. This result indicates that TPPCN could be a potential anti-Gram-positive bacteria drug.

Images of plates used for the quantification of the killing effect on *S. epidermidis* and *E. coli* are shown in Figs. 21A-21F and 22A-22F. Without treatment, the bacteria grow healthily on the plate. Light irradiation alone decreases the amount of *S. epidermidis* to some extent, and does not exert an obvious effect on *E.coli* viability. Treatment with TPPCN alone decreases the amount of *S. epidermidis* growth to a great extent, but there are some living bacteria are present that can grow to form colonies on the plate, suggesting a killing effect of TPPCN on *S. epidermidis* in the dark. In contrast, the mere presence of TPPCN does not exert an obvious effect on *E.coli* viability (Fig. 22E). In the presence of both TPPCN and light irradiation, *S. epidermidis* is killed effectively and almost no colonies form on the plate, which is a good sign of high *S. epidermidis* killing efficiency under light irradiation (Figs. 21C and 22C). In contrast, TPPCN and light irradiation do not appear to impair *E.coli*colony formation (Figs. 21F and 22F). These results prove that TPPCN alone can preferentially kill Gram-positive bacteria over Gram-negative bacteria, and could be more efficient together with light irradiation.

Example 9

Theranostic Potential of TPPCN (and AIE luminogen)

Further application of TPPCN to complex system including cells and bacteria was investigated. As illustrated in Figs. 23A-23C,TPPCN can selectively stain HeLa cells and *S. epidermidis* over MDCK-II cells. After white light illumination, HeLa cells and *S. epidermidis* are selectively killed by the TPPCN sensitized ROS generation (Fig. 24A-24C). Evidently, TPPCN is capable of selectively imaging cancer cells and Gram-positive bacteria as well as selectively killing them with the aid of light illumination. These properties can be of great value, especially in the exploration of TPPCN as part of a theranostic system.

Example 10

Photophysical Properties of TPE-CP

The UV-vis absorption spectrum of TPE-CP was recorded in DCM solution and is shown in Fig. 25. TPE-CP shows an absorption maximum at 475 nm located in the visible light range, which is friendly for biological system against UV excitation. TPE-CP inherits the AIE feature, as evidenced by the photoluminescence (PL) spectra measured in the solution and aggregate states (Figs. 26A-26B). TPE-CP emits faintly in pure DCM solution. The intensity increases gradually with the adding of hexane, a poor solvent for the luminogen. The quantum yield (QY) in pure DCM and in the DCM/hexane mixture (1: 99, v/v) was 0% and 6.7%. Clearly, the PL and QY results demonstrate that TPE-CP is AIE-active.

Example 11

TPE-CP Biocompatibility

The biocompatibility of TPE-CP was evaluated using the 3-(4,5-dimethyl-2-thiazolyl)-2,5-diphenyltetrazolium bromide (MTT) assay. As depicted in Fig. 27, no significant change in cell viability is observed when the HeLa cells are cultured in the presence of different concentrations of TPE-CP, up to 50μM for 24 h. This reveals that TPE-CP shows no cytotoxicity and good biocompatibility to HeLa cells.

Example 12

TPE-CP Lipid Droplet Targeting

HeLa cells were used as a cell model and were co-stained with TPE-CP (10 μM) for 30 min and BODIPY 493/503 (1 μg/ml) for 15 min. As shown in Figs. 28A-28C, orange fluorescence from TPE-CP and green fluorescence from BODIPY 493/503 are readily observed. The correlation coefficient for these two images is calculated to be 94%, suggesting that TPE-CP can specifically target lipid droplets.

Example 13

TPE-CP Photostability

As one of the key criteria for evaluating a fluorescent visualizer, the photostability of TPE-CP was assessed by sequential scanning with a confocal microscope. More than 40% of the

fluorescence of BODIPY 493/503 is lost after 50 scans (Figs. 29A-29B). TPE-CP fluorescence can still be observed in lipid droplets clearly, and more than 80% signal of TPE-CP is retained after 50 scans (Figs. 29A-B). Evidently, TPE-CP shows a much higher photostability than BODIPY 493/503.

Example 14

TPE-CP ROS Generation

TPE-CP is also a photosensitizer for ROS generation. Since TPE-CP absorbed strongly in the visible light region, white light was used as the excitation light source. H2DCF-DA, which emits fluorescence at around 530 nm in the presence of ROS, was used as a ROS indicator. In the presence of TPE-CP, the fluorescence of H2DCF-DA is gradually enhanced with increase dirradiation time (Fig. 30A). After 10 min exposure to white light, the intensity of H2DCF-DA was almost 670 times higher than the original emission intensity without light irradiation. Such change, however, was not observed in TPE-CP or H2DCF-DA alone. The ROS generation efficiency of TPE-CP inside the cells was then investigated. Before 405 nm laser irradiation, almost no emission from H2DCF-DAcould be detected in the cells (Fig. 30B). After 405 nm laser irradiation for 30 s, the green emission of H2DCF-DA was observed (Fig. 30C). For cells incubated with H2DCF-DA alone, the emission remains faint both before and after 405 nm laser irradiation (Figs. 30D and 30E). The results indicate that TPE-CP could serve as a sensitizer for ROS generation both in solution and in cells.

Example 15

TPE-CP Selective Imaging and Killing of Gram Positive Bacteria

Similar to the difference of MMP of cancer cells and normal cells, Gram-positive bacteria have much more negative charge than Gram-negative bacteria due to the teichoic acid found on the Gram-positive bacterial membrane. Therefore, TPE-CP was applied to bacterial differentiation imaging. For biosafety the nonpathogenic bacteria *S. epidermidis* and *E.coli* were selected as representative species for this study. As shown in Figs. 31A-31D, after incubation with 10 μM TPE-CP for 30 min, only Gram-positive bacteria, *S. epidermidis*, can be visualized. Gram-negative bacteria, *E. coli*, can't be observed clearly, indicating TPE-CP stains only Gram-positive bacteria. This result was confirmed in the co-culture system of Gram-positive bacteria

and Gram-negative bacteria.

The antibiosis capability of TPE-CP was further explored. The optical density (OD600) change of bacteria incubated with TPE-CP was investigated. As illustrated in Figs. 32A and 32B, TPE-CP exhibits an obvious inhibition effect on the proliferation of *S. epidermidis*. The time-dependent and concentration-dependent OD600 changes of *S. epidermidis* incubated with TPPCN are shown in Figs. 33A and 33B, respectively. According to the curve plotted by concentration-dependent OD600 changes incubated with TPPCN (Figs. 33C and 33D), the IC_{50} of TPE-CP for inhibition of *S. epidermidis* growth is estimated to be 3.144 μM. This result indicates that TPE-CP could be a potential anti-Gram-positive bacteria drug.

Images of plates used for quantification of the killing effect on *S. epidermidis* and *E. coli* are shown in Figs. 34A-34H. Without treatment, the bacteria grow healthily on the plate. Light irradiation alone decreases the amount of *S. epidermidis* to some extent, and does not exert an obvious effect on *E. coli* viability. Treatment with TPE-CP alone can kill *S. epidermidis* effectively (Fig. 34C). Treatment with TPE-CP alone does not exert an obvious effect on *E.coli* viability (Fig. 34E). In the presence of both TPE-CP and light irradiation, *S. epidermidis* is killed much more effectively and almost no colonies form on the plate, which is a good sign of high *S. epidermidis* killing efficiency under light irradiation (Fig. 34C). In contrast, TPE-CP and light irradiation do not appear to impair *E.coli* colony formation (Fig. 34H). These results prove that TPE-CP alone can kill Gram-positive bacteria, and could be more efficient together with light irradiation.

The morphology of bacteria, which indicates bacteria viable state, was then investigated by scanning electron microscopy (SEM). As shown in Fig. 35A, without treatment, the morphology of *S. epidermidis* remains regular with clear borders and smooth bodies. When bacteria overlap with each other, a well-defined border can be clearly resolved, indicating the healthy state of the bacteria. After treatment, however, bacteria shrank and fusion took place, resulting in enormous changes in morphology(Fig. 35B). The SEM results clearly demonstrate that the presence of TPE-CP and light together can lead to bacteria death characterized by the morphological changes.

The present subject matter being thus described, it will be apparent that the same may be modified or varied in many ways. Such modifications and variations are not to be regarded as a

departure from the spirit and scope of the present subject matter, and all such modifications and variations are intended to be included within the scope of the following claims.

We Claim:

1. An AIE luminogen probe comprising a compound having a chemical structure selected from the group consisting of:

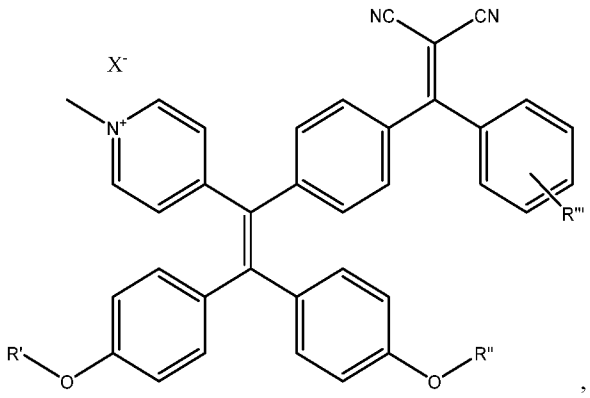

,

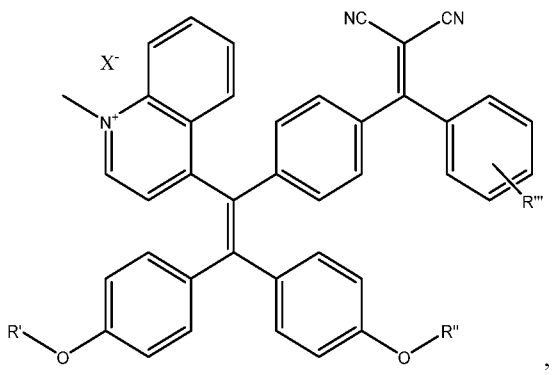

,

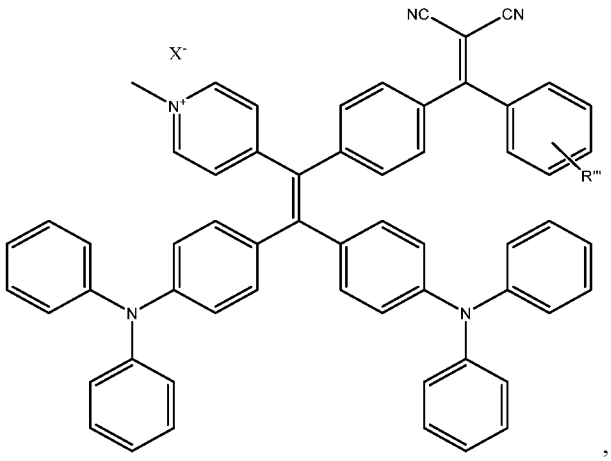

,

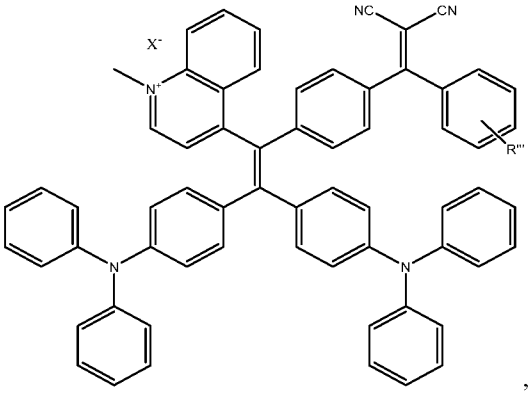

,

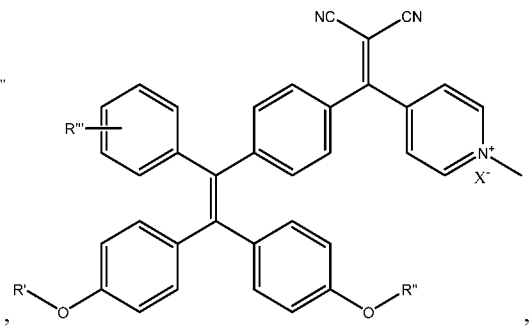

,

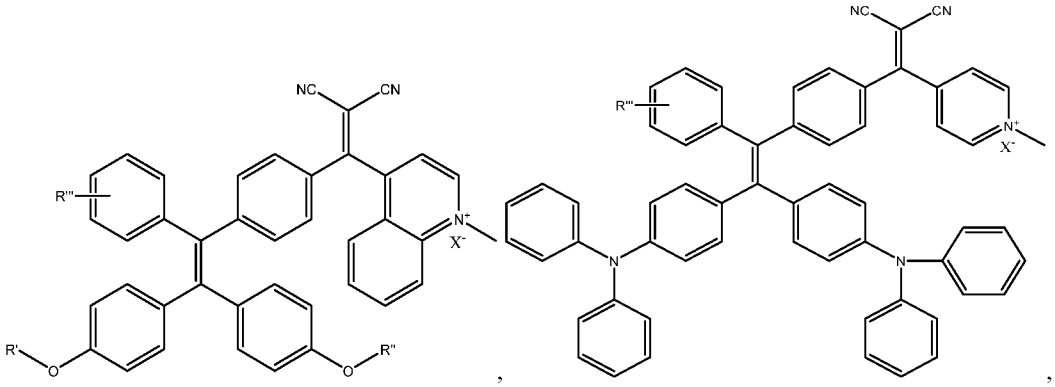

, and

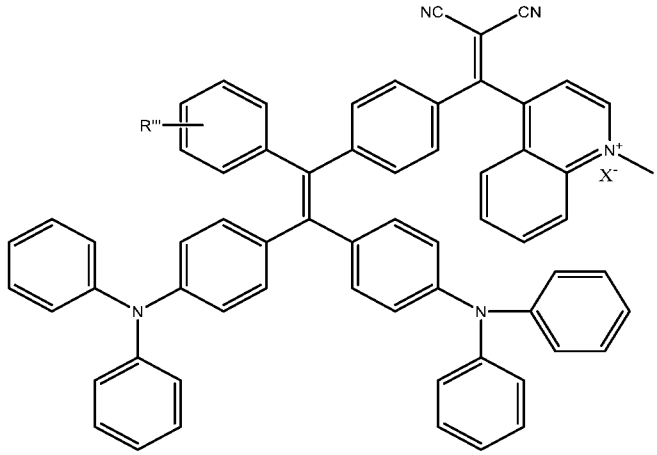

;

wherein R', R", and R"' are independently selected from the group consisting of H, alkyl, unsaturated alkyl, heteroalkyl, cycloalkyl, heterocycloalkyl, aryl, heteroaryl, alkyl-NCS, alkyl-N_3, and alkyl-NH_2; and

wherein the counteranion X^- is selected from the group consisting of I^-, PF_6^-, BF_4^-, SbF_6^-, SbF_5^-, CH_3COO^-, CF_3COO^-, CO_3^{2-}, SO_4^{2-}, SO_3^{2-}, $CF_3SO_2^-$, TsO^-, ClO_4^-, F^-, Cl^-, Br^-, $(F_3CSO_2)N^-$, and PO_4^{3-}.

2. The AIE luminogen probe of claim 1 wherein the compound has a chemical structure selected from the group consisting of:

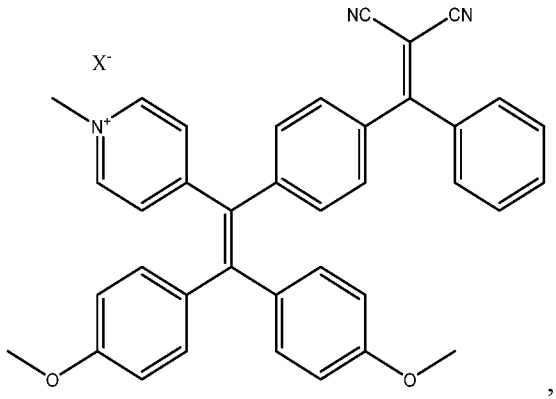

, and

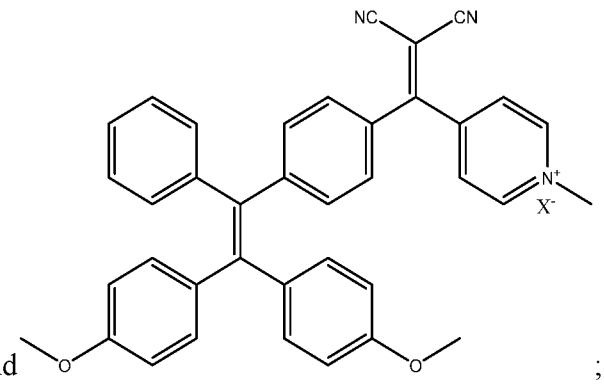

;

(TPPCN) (TPE-CP)

wherein the counteranion X^- is selected from the group consisting of I^- and PF_6^-.

3. The AIE luminogen probe of claim 1, wherein the probe exhibits mitochondria selective staining.

4. The AIE luminogen probe of claim 1, wherein the probe exhibits lipid droplet specific staining.

5. The AIE luminogen probe of claim 1, wherein the probe exhibits cancer cell specific staining.

6. The AIE luminogen probe of claim 5, wherein the cancer cells are HeLa cells.

7. The AIE luminogen probe of claim 1, wherein the probe exhibits gram-positive bacteria specific staining.

8. The AIE luminogen probe of claim 7, wherein the gram-positive bacteria is *S. epidermidis*.

9. The AIE luminogen probe of claim 1, wherein the probe generates reactive oxygen species (ROS) upon light irradiation.

10. The AIE luminogen probe of claim 1, wherein the probe is a photosensitizer.

11. The AIE luminogen probe of claim 1, wherein the probe is used for treating as well as imaging cancer cells.

12. The AIE luminogen probe of claim 1, wherein the probe is used for treating as well as imaging gram positive bacteria.

13.An AIE luminogen probe comprising a compound having a chemical structure selected from the group consisting of:

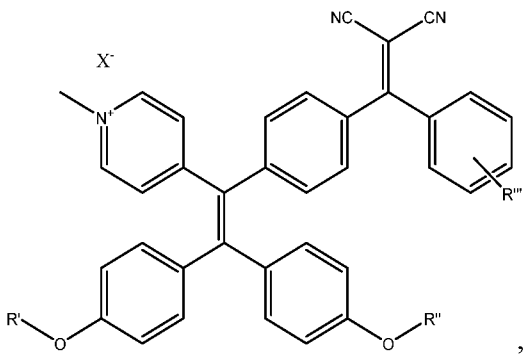

, and

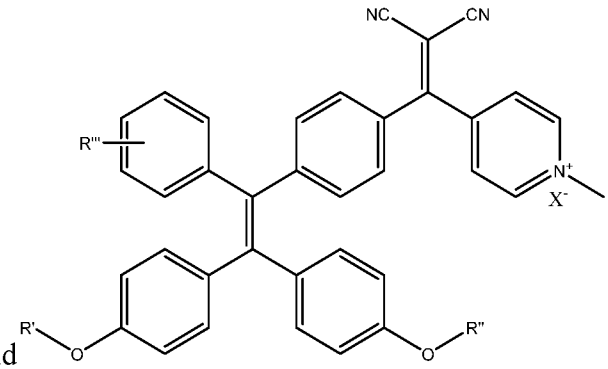

;

wherein R', R", and R"' are independently selected from the group consisting of H, alkyl, unsaturated alkyl, heteroalkyl, cycloalkyl, heterocycloalkyl, aryl, heteroaryl, alkyl-NCS, alkyl-N_3, and alkyl-NH_2; and

wherein the counteranion X^- is selected from the group consisting of I^-, PF_6^-, BF_4^-, and SbF_6^-.

14. The AIE luminogen probe of claim 13 wherein the compound has a chemical structure selected from the group consisting of:

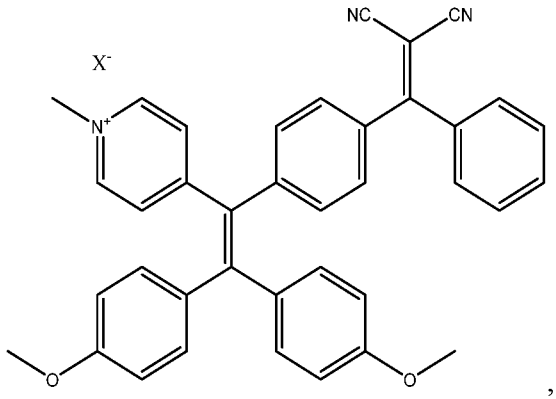

, and

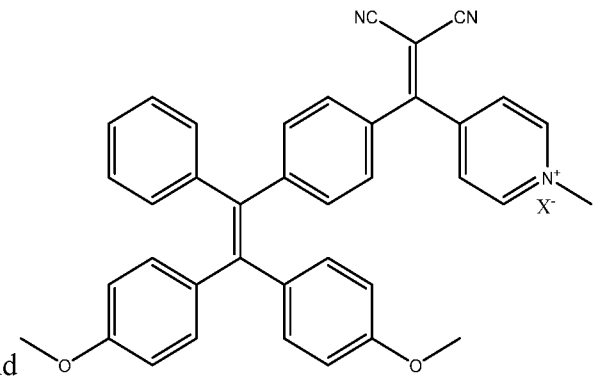

;

(TPPCN) (TPE-CP)

wherein the counteranion X^- is selected from the group consisting of I^- and PF_6^-.

15. A method of locating harmful cells in a patient, comprising:

administering the AIE luminogen probe of claim 1 to the patient; and

locating the harmful cells using fluorescent imaging.

16. The method of claim 15, wherein the harmful cells are cancer cells.

17. The method of claim 15, wherein the harmful cells are gram-positive bacterial cells.

18. The method of claim 15, wherein the AIE luminogen probe is administered to a surgical site.

19. The method of claim 15, wherein the harmful cells are quantified by observing emission intensity.

20. A method of stopping or inhibiting growth of harmful cells in a patient, comprising:

administering the AIE luminogen probe of claim 1 to the patient;

locating the harmful cells using fluorescent imaging; and

subjecting the site of the harmful cells to white light irradiation while the AIE luminogen probe is present at the site of the harmful cells to stop or inhibit the growth of the harmful cells.

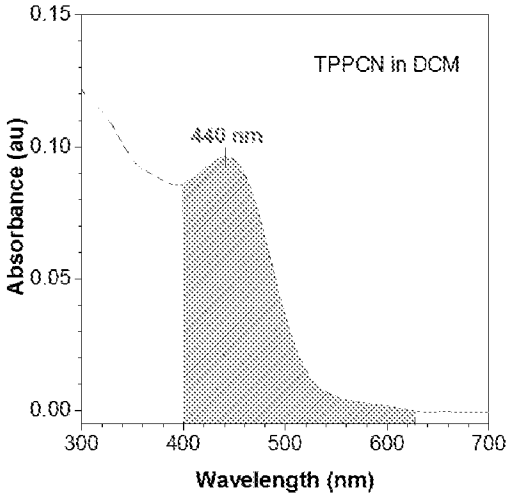

FIG. 1

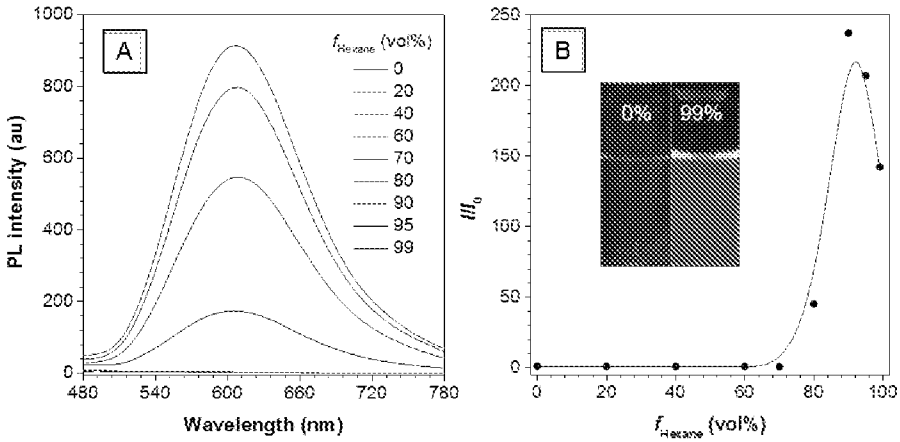

FIGs. 2A-2B

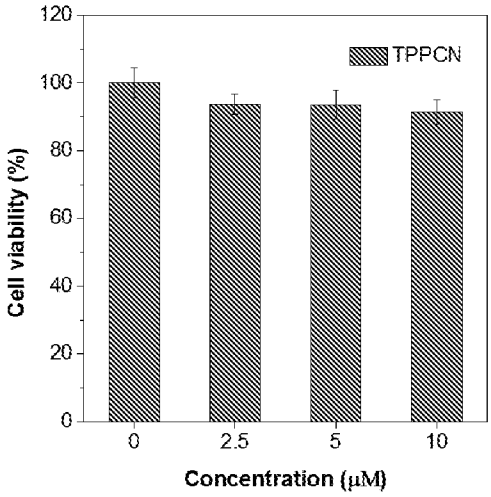

FIG. 3

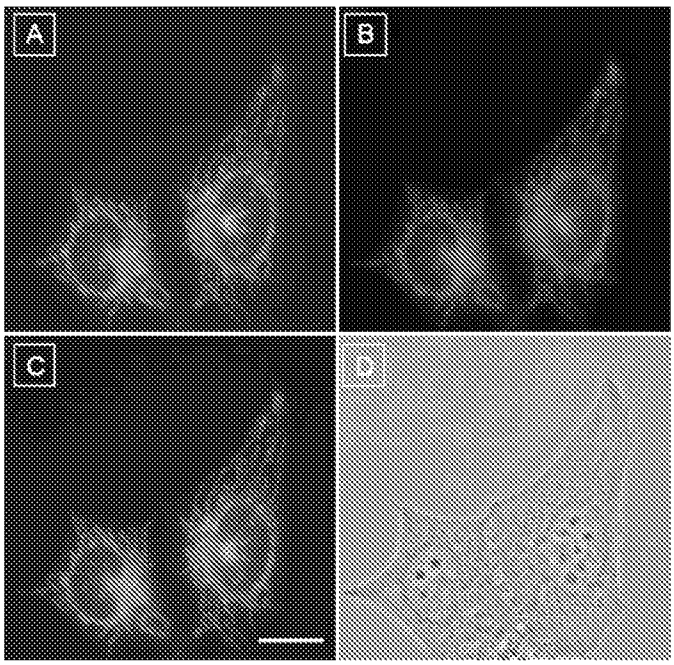

FIGs. 4A-4D

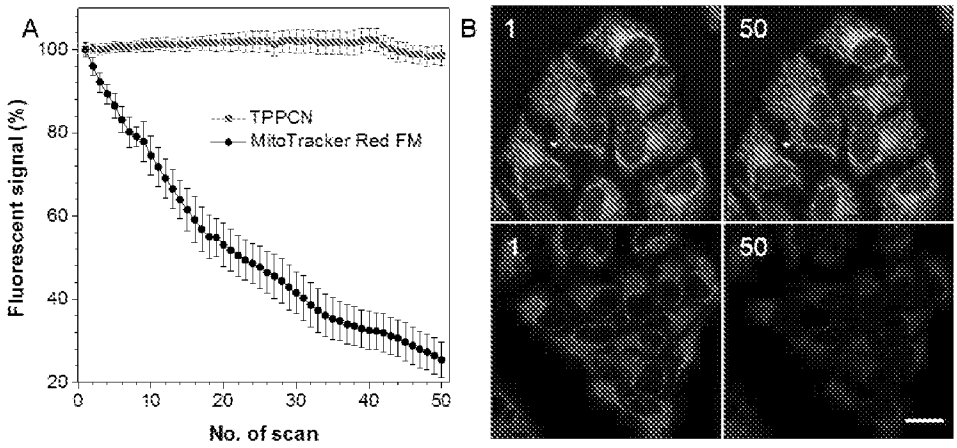

FIGs. 5A-5B

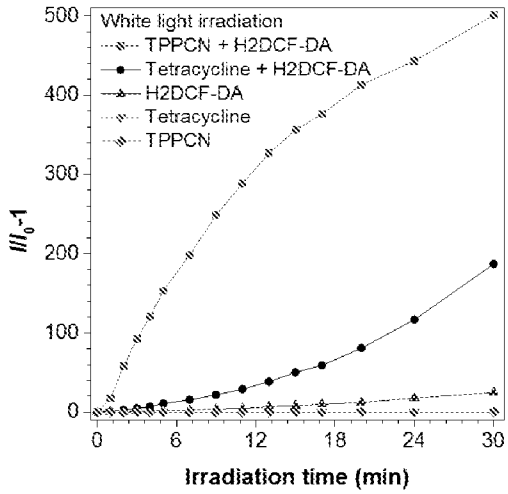

FIG. 6

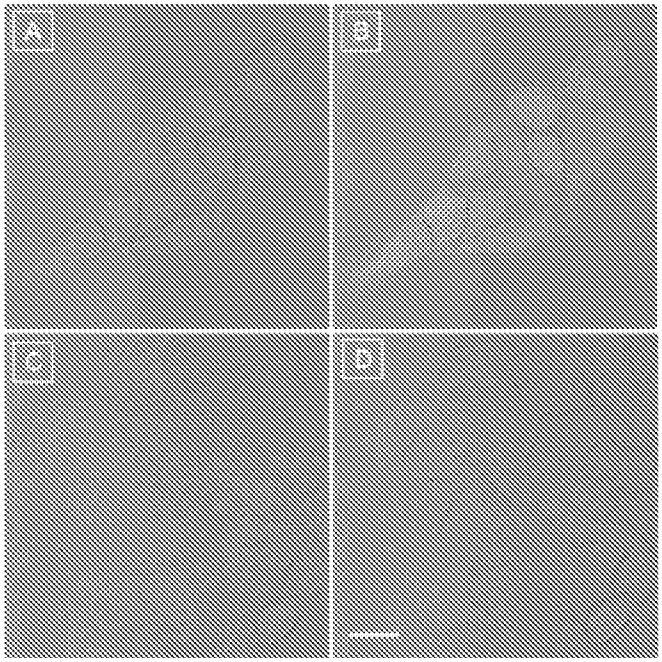

FIGs. 7A-7D

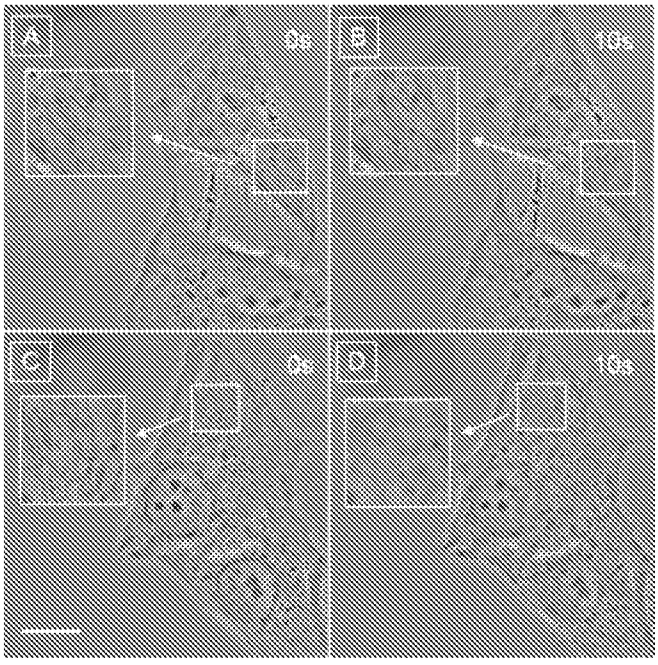

FIGs. 8A-8D

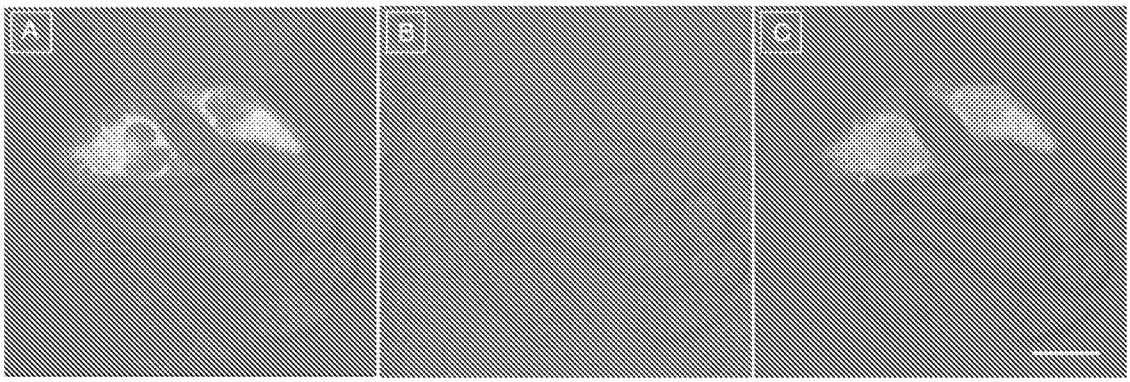

FIGs. 9A-9C

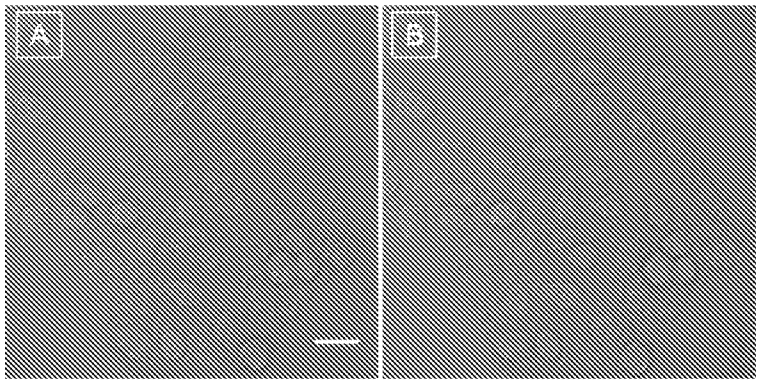

FIGs. 10A-10B

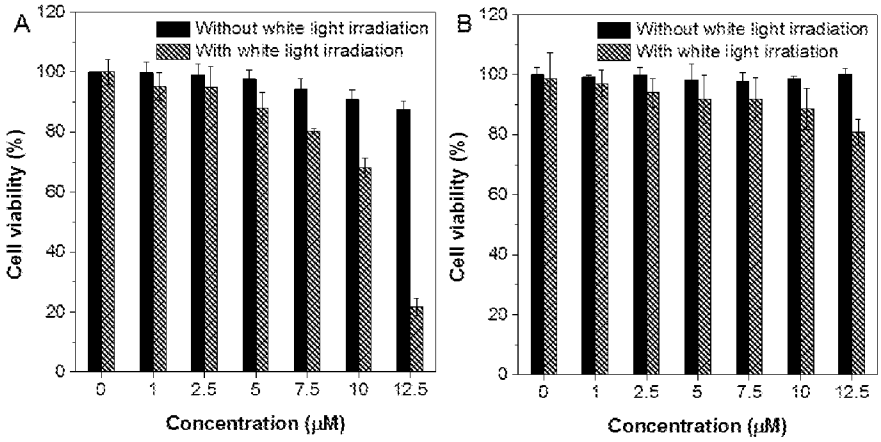

FIGs. 11A-11B

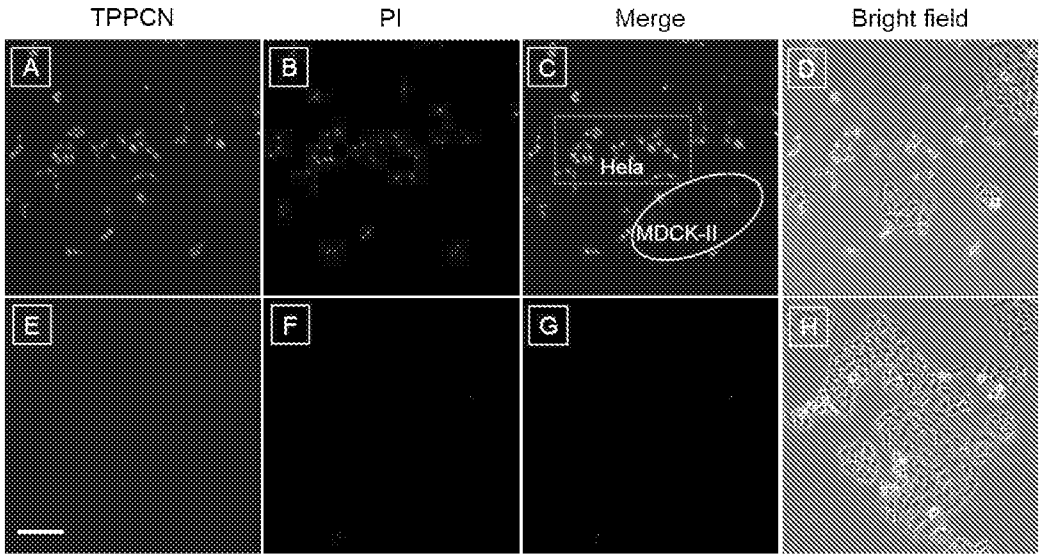

FIGs. 12A-12H

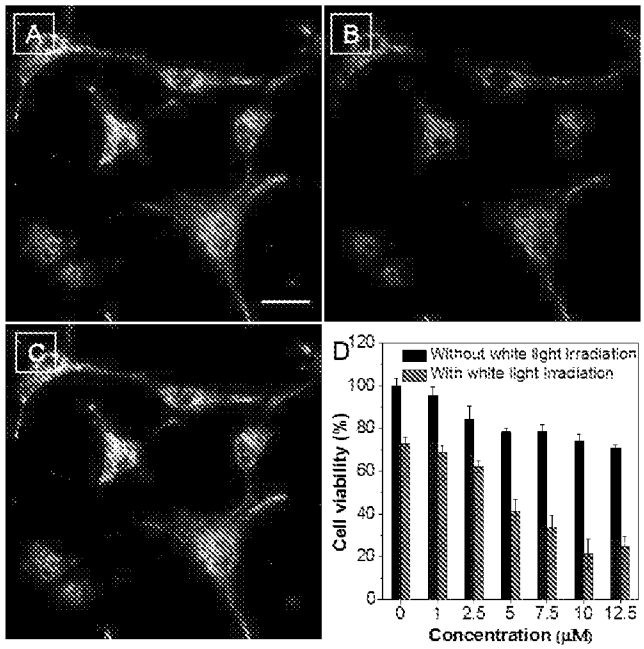

FIGs. 13A-13D

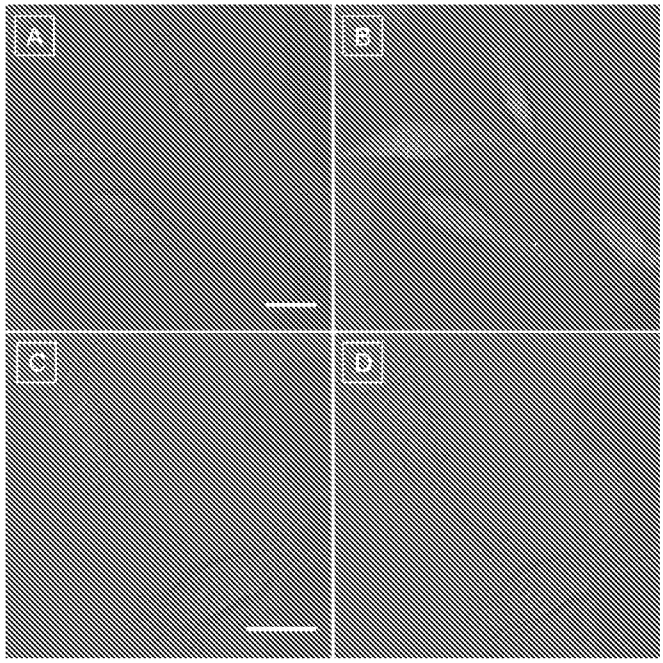

FIGs. 14A-14D

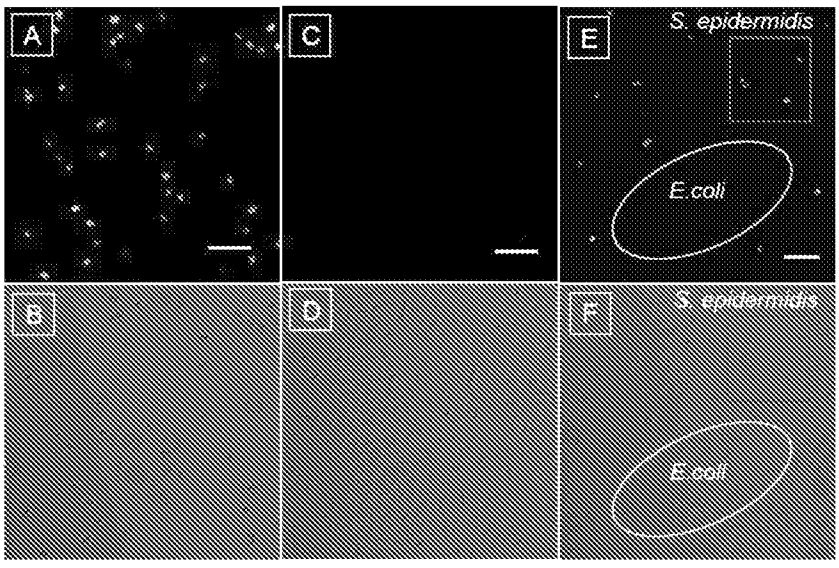

FIGs. 15A-15F

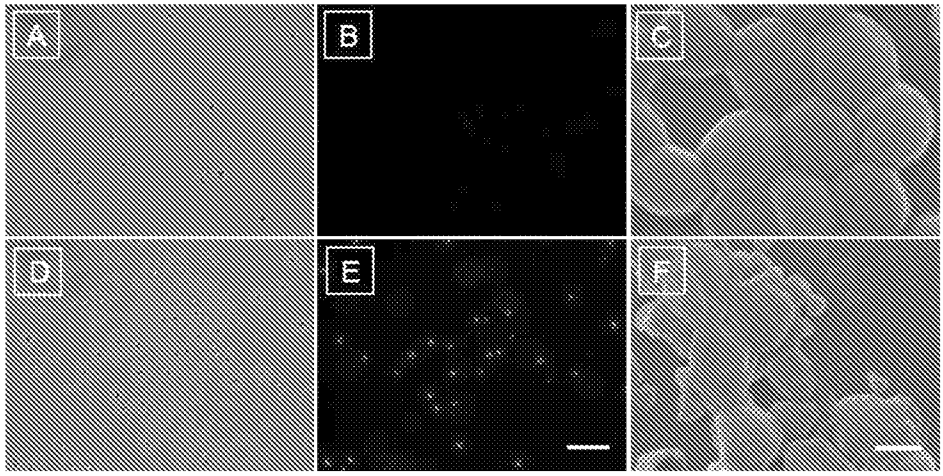

FIGs. 16A-16F

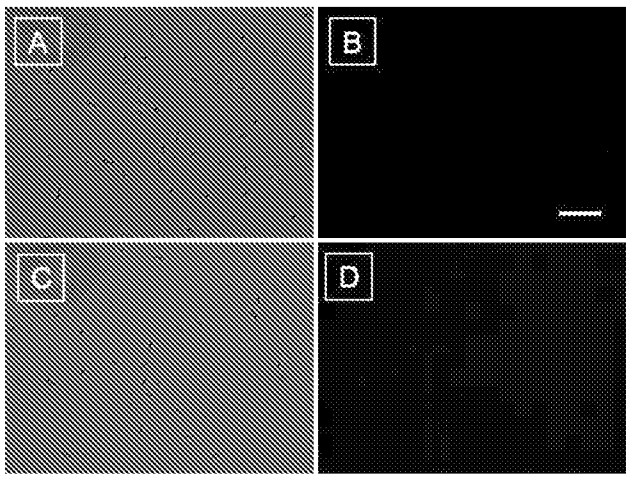

FIGs. 17A-17D

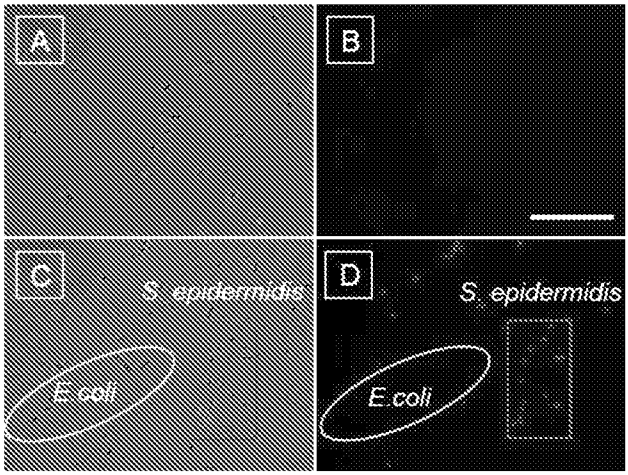

FIGs. 18A-18D

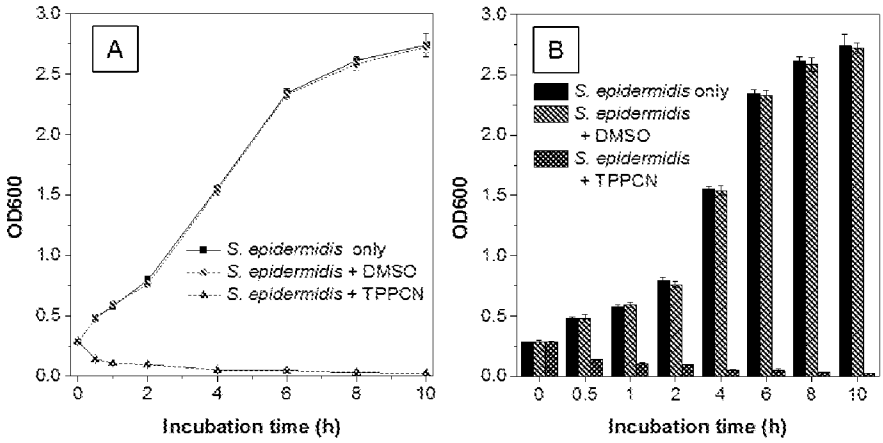

FIGs. 19A-19B

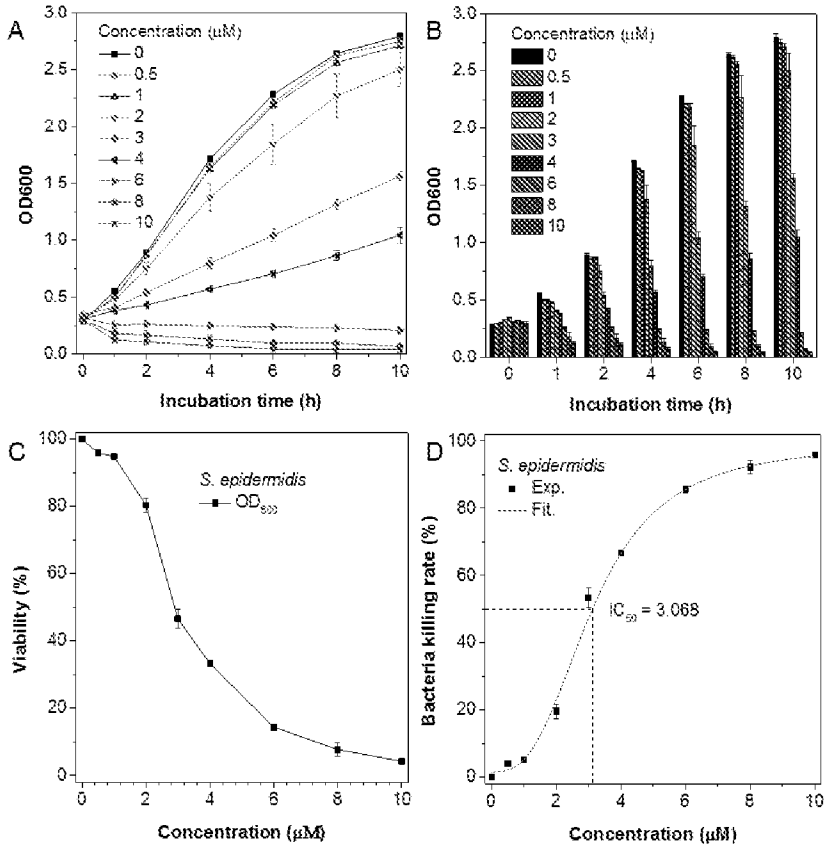

FIGs. 20A-20D

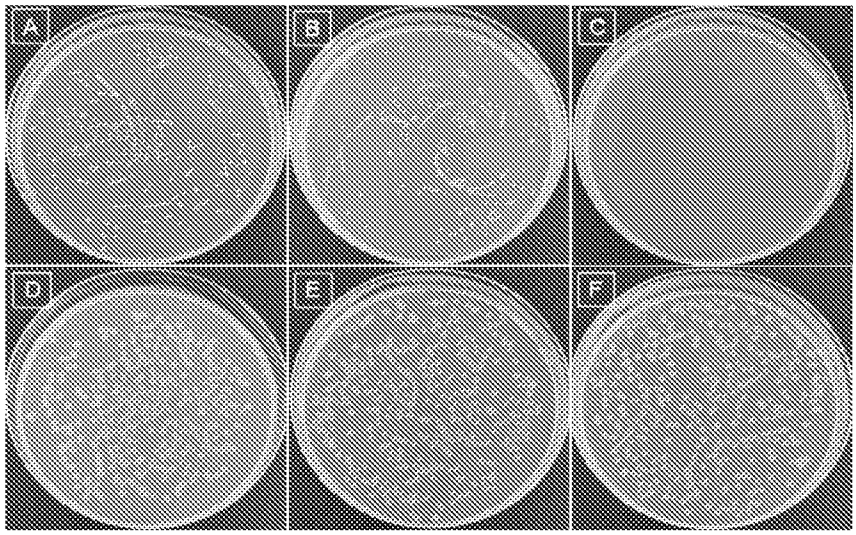

FIGs. 21A-21F

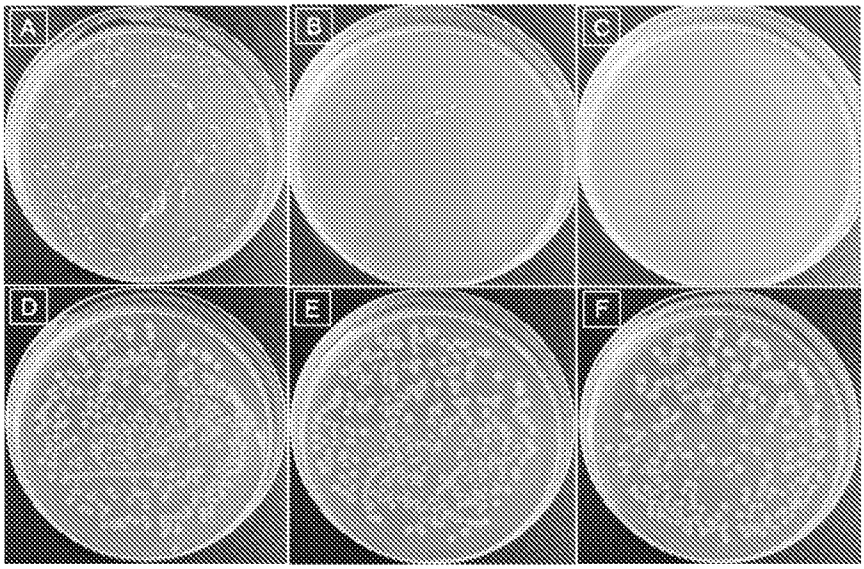

FIGs. 22A-22F

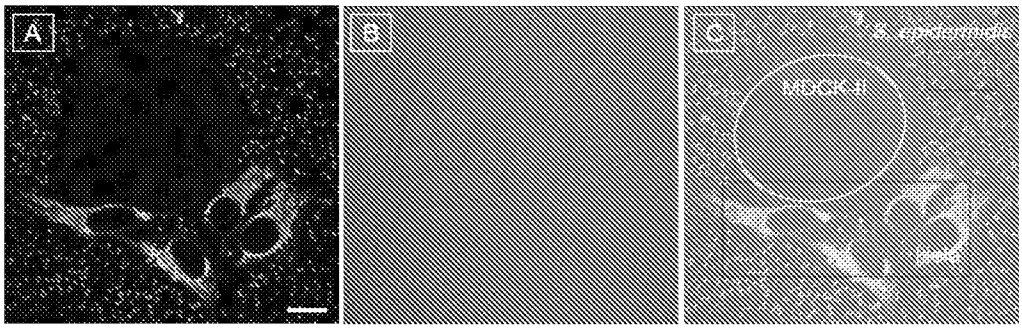

FIGs. 23A-23C

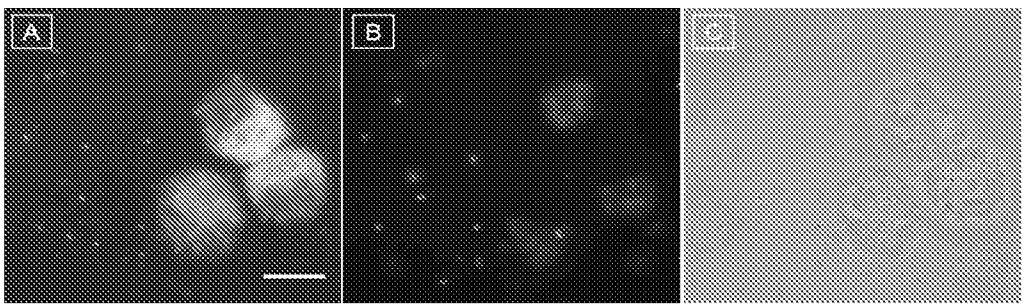

FIGs. 24A-24C

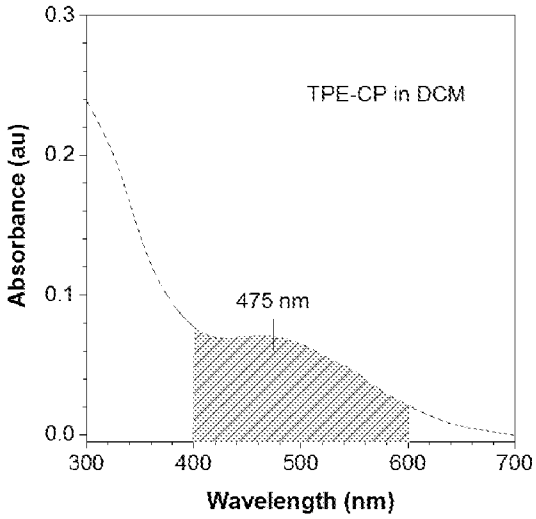

FIG. 25

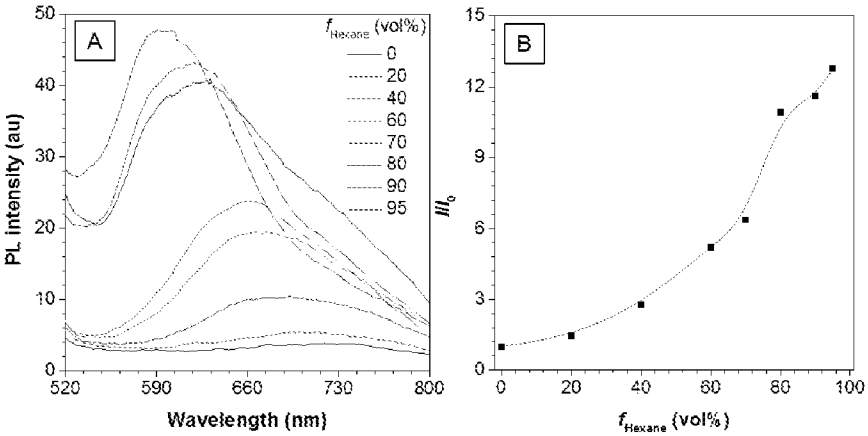

FIGs. 26A-26B

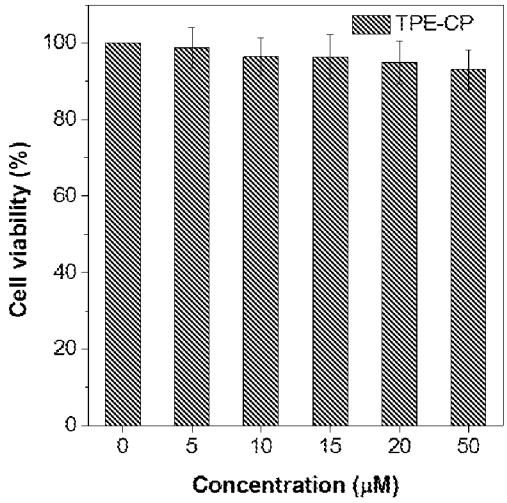

FIG. 27

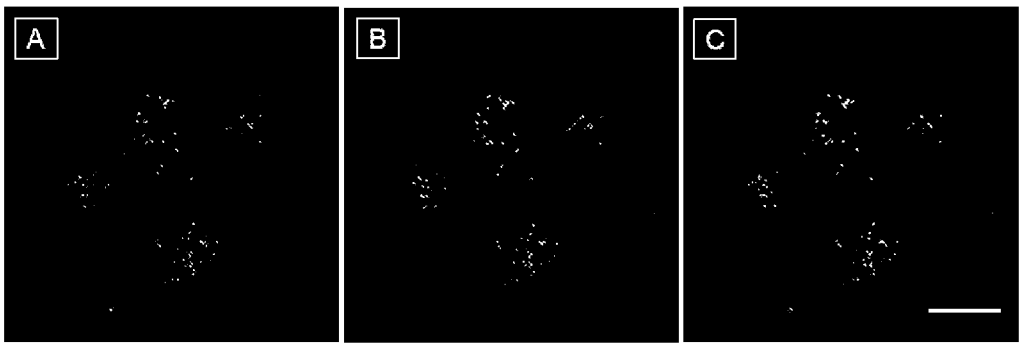

FIGs. 28A-28C

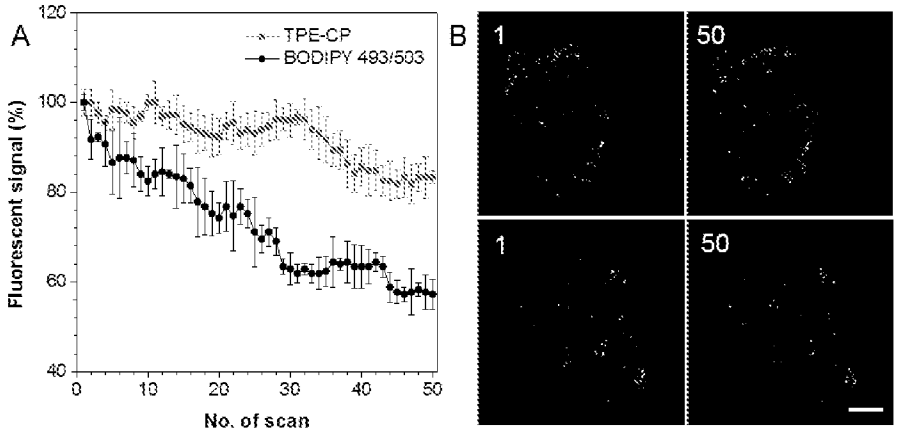

FIGs. 29A-29B

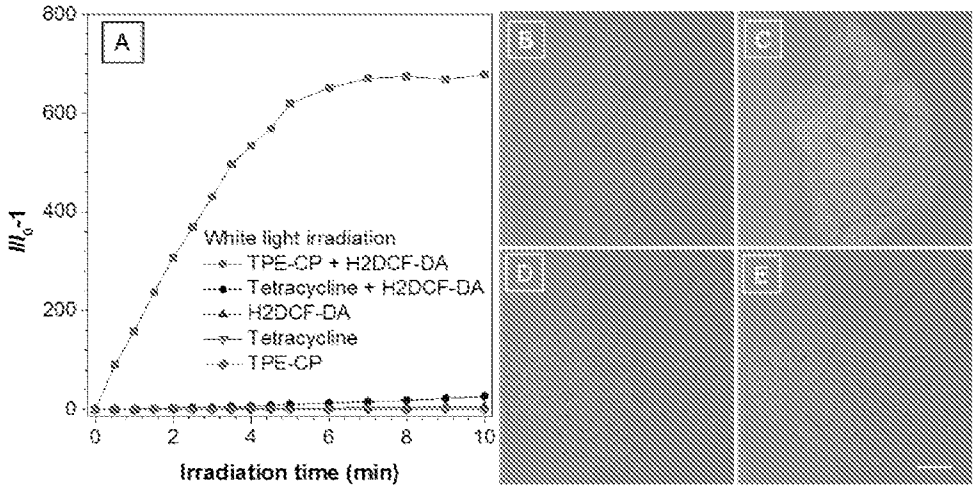

FIGs. 30A-30E

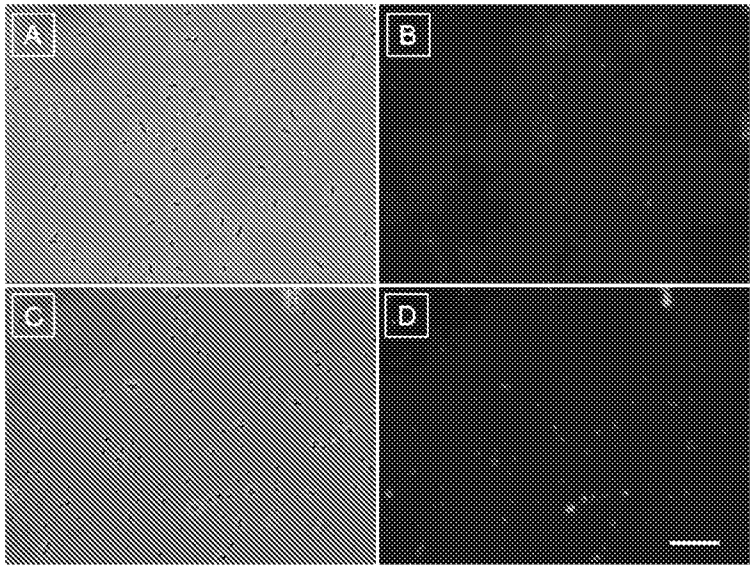

FIGs. 31A-31D

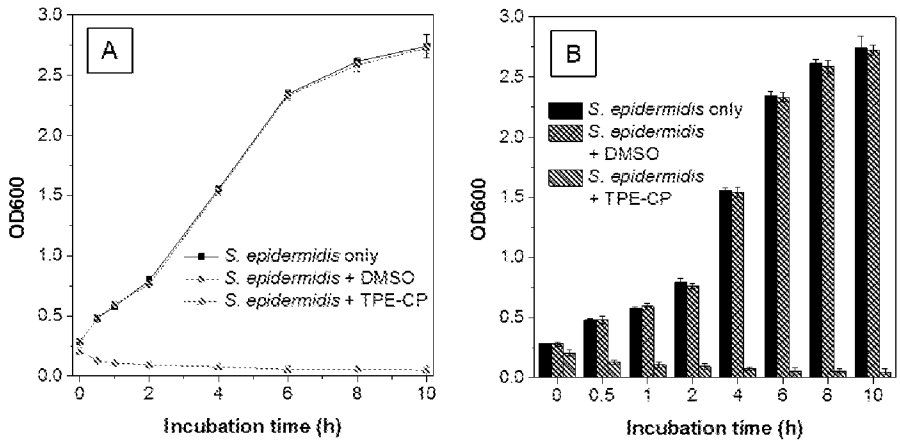

FIGs. 32A-32B

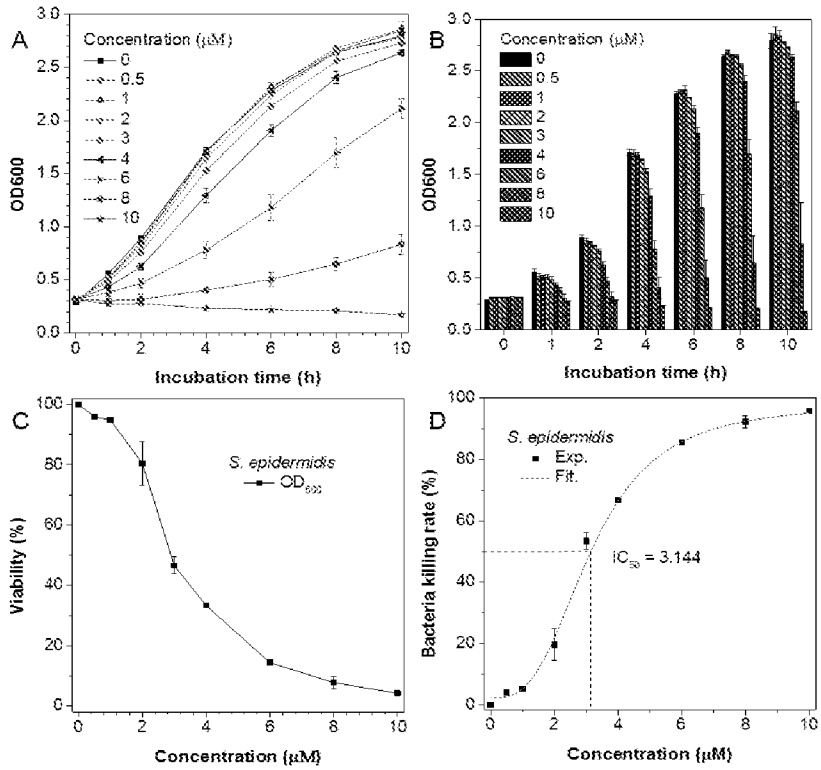

FIGs. 33A-33D

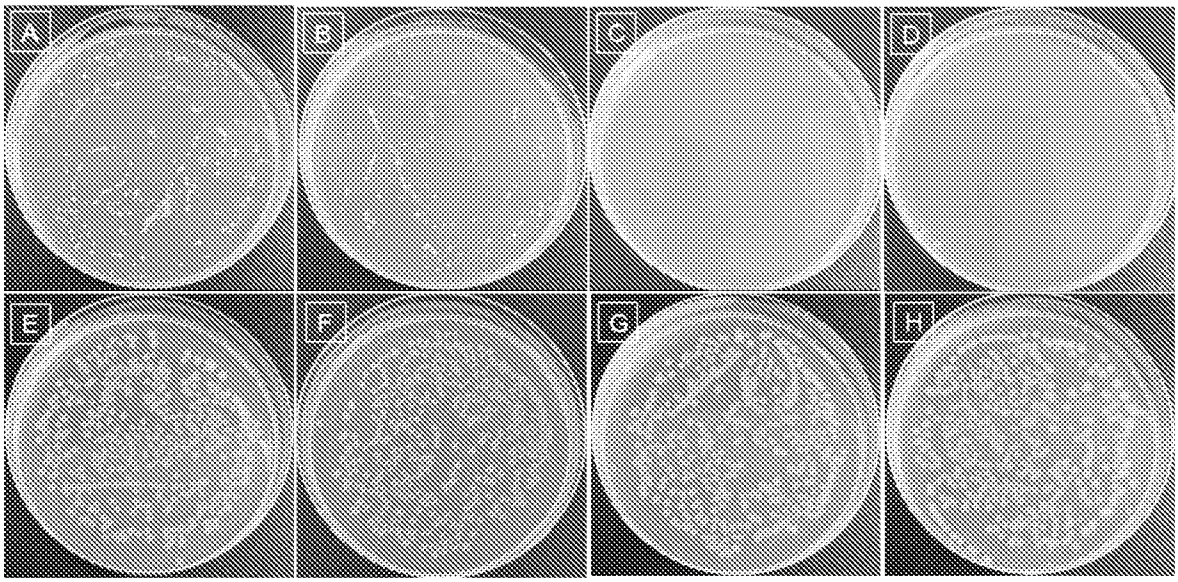

FIGs. 34A-34H

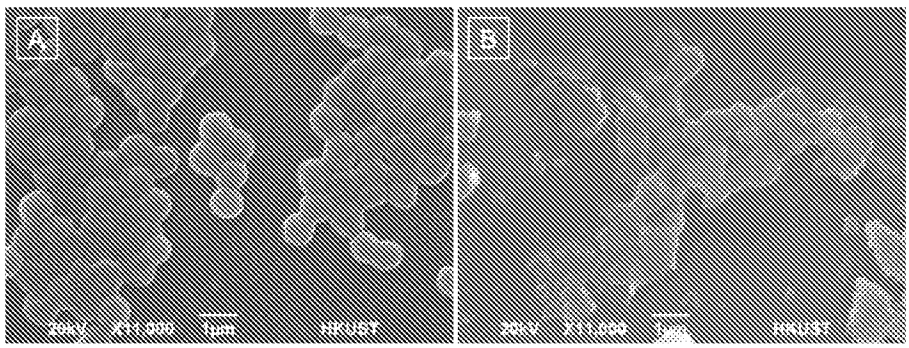

FIGs. 35A-35B

INTERNATIONAL SEARCH REPORT

International application No.
PCT/CN2018/087479

A. CLASSIFICATION OF SUBJECT MATTER

C07D 215/42(2006.01)i; C07D 215/26(2006.01)i; C07D 213/30(2006.01)i; A61K 31/44(2006.01)i; A61K 31/438(2006.01)i; C09K 11/06(2006.01)i; G01N 21/64(2006.01)i; A61P 31/04(2006.01)i; A61P 35/00(2006.01)i

According to International Patent Classification (IPC) or to both national classification and IPC

B. FIELDS SEARCHED

Minimum documentation searched (classification system followed by classification symbols)

C07D; A61K; C09K; G01N; A61P

Documentation searched other than minimum documentation to the extent that such documents are included in the fields searched

Electronic data base consulted during the international search (name of data base and, where practicable, search terms used)

CNPAT, CNKI, WPI, EPODOC, REGISTRY, CAPLUS Hong Kong University of Science and Technology, Tang Benzhong, Kang Miaomiao, Gu Xinggui, tetraphenylethene, TPE, luminogen, AIEgens, AIE, aggregation-induced emission, fluorescen?, photodynamic, STN structure search

C. DOCUMENTS CONSIDERED TO BE RELEVANT

Category*	Citation of document, with indication, where appropriate, of the relevant passages	Relevant to claim No.
Y	WO 2015163817 A1 (UNIV SINGAPORE ET AL.) 29 October 2015 (2015-10-29) description paragraphs [00177], [00178], [00184], [00187]	1-20
Y	WO 2016070854 A1 (TANG BENZHONG) 12 May 2016 (2016-05-12) claims 1-4	1-20
Y	WO 2016078603 A1 (UNIV HONG KONG SCIENCE & TECHN) 26 May 2016 (2016-05-26) claims 1, 13, 14, 17	1-20

☐ Further documents are listed in the continuation of Box C. ☑ See patent family annex.

* Special categories of cited documents:

"A" document defining the general state of the art which is not considered to be of particular relevance

"E" earlier application or patent but published on or after the international filing date

"L" document which may throw doubts on priority claim(s) or which is cited to establish the publication date of another citation or other special reason (as specified)

"O" document referring to an oral disclosure, use, exhibition or other means

"P" document published prior to the international filing date but later than the priority date claimed

"T" later document published after the international filing date or priority date and not in conflict with the application but cited to understand the principle or theory underlying the invention

"X" document of particular relevance; the claimed invention cannot be considered novel or cannot be considered to involve an inventive step when the document is taken alone

"Y" document of particular relevance; the claimed invention cannot be considered to involve an inventive step when the document is combined with one or more other such documents, such combination being obvious to a person skilled in the art

"&" document member of the same patent family

Date of the actual completion of the international search	Date of mailing of the international search report
05 August 2018	**23 August 2018**

Name and mailing address of the ISA/CN	Authorized officer
STATE INTELLECTUAL PROPERTY OFFICE OF THE P.R.CHINA **6, Xitucheng Rd., Jimen Bridge, Haidian District, Beijing 100088** **China**	**LIU,Peng**
Facsimile No. **(86-10)62019451**	Telephone No. **62411191**

INTERNATIONAL SEARCH REPORT

International application No.
PCT/CN2018/087479

Box No. II Observations where certain claims were found unsearchable (Continuation of item 2 of first sheet)

This international search report has not been established in respect of certain claims under Article 17(2)(a) for the following reasons:

1. ☑ Claims Nos.: **15-20**
because they relate to subject matter not required to be searched by this Authority, namely:

[1] These claims are characterized as methods for diagnosing or treating diseases (PCT Rule 39.1(iv)), but the search has been carried out and based on the use of compound in manufacture of medicaments for diagnosing or treating corresponding diseases.

2. ☐ Claims Nos.:
because they relate to parts of the international application that do not comply with the prescribed requirements to such an extent that no meaningful international search can be carried out, specifically:

3. ☐ Claims Nos.:
because they are dependent claims and are not drafted in accordance with the second and third sentences of Rule 6.4(a).

INTERNATIONAL SEARCH REPORT
Information on patent family members

International application No.
PCT/CN2018/087479

Patent document cited in search report	Publication date (day/month/year)	Patent family member(s)	Publication date (day/month/year)
WO 2015163817 A1	29 October 2015	US 2017168041 A1	15 June 2017
		CN 106470964 A	01 March 2017
WO 2016070854 A1	12 May 2016	None	
WO 2016078603 A1	26 May 2016	CN 107001927 A	01 August 2017